A. THE IUCF COOLER PROJECT

A.1. Introduction

The period from April 1987 through April 1988 represents an extraordinarily fruitful year for the IUCF Cooler project. Not only did most of the critical installation work take place within the first half of this period, but the initial operation of the essentially completed ring during the second half of this period successfully demonstrated its function as a beam storage ring, as a synchrotron accelerator, as an electron Cooler, and as an internal target scattering facility.

These achievements in both ring construction and ring commissioning are the result of dedicated efforts by a lot of people working under an ambitious and demanding time schedule. Their contribution to this major new IUCF facility is appreciated and gratefully acknowledged; each participant in this undertaking can be justifiably proud of his or her accomplishments!

Two highlights of this past year stand out above the multitude of others. One is the symbolic changeover from ring construction to ring operation which occurred on October 30, when beam was carried around one full turn of the just-closed ring for the first time. The other was the turnon of the electron cooling system in the ring and the achievement of beam cooling in mid-April of this year. Together, these two events mark the turning of a dream of an IUCF electron-cooled storage ring into a reality.

Many important milestones were passed on the way to achieving this reality, of course. They are reviewed in the following sections of this report, starting with an account of the final phases of Cooler construction in Sect. A.2. The initial six months of Cooler commissioning are detailed in Sect. A.3., beginning with a chronological record of the many highlights followed by more detailed descriptions of beam injection, storage, acceleration and cooling. Technical details of the electron cooling and beam diagnostics subsystems can be found in Sects. A.4. and A.5., respectively, along with representative results. Sections A.6. through A.9. deal briefly with developments in the Cooler areas.

The Cooler is now entering an intensive period of multifaceted operation. The Cooler running time will be divided among commissioning of new operating modes, machine studies, performance improvements, startup of early internal target experiments, operator training, and the like.

There will be further explorations of tune space and aperture limits, as well as acceleration of cooled beam to higher energies, time-shared with further tests of the G-region gas jet target and detector setup to study and solve the vexing problem of beam halo producing high background rates.

In May we will have a run which uses high-intensity pulses of protons from the "stripper loop" to set up the ring for non-stripping, one-turn ferrite kicker injection and storage, then switch to the low-intensity polarized proton beam at the same energy to carry out depolarization studies and test the "Siberian Snake" concept of polarization control (Experiment CE-05; the G-region target and detectors serve as a high-efficiency polarimeter in these tests).

Once cooled beam at 287 MeV is achieved and the beam halo problem resolved,

first trials of the NN pion threshold experiment (CE-01) will be interspersed with further machine studies. We are, of course, particularly interested in learning as much as we can about the evolution of the beam phase space distribution under various combinations of electron cooling, target heating, and rf manipulation. This stage of testing will continue for the rest of the year, at a rate determined primarily by beam availability.

A.2. Cooler Construction, T. Sloan, M. Wedekind, B. Palmer, R. Stillabower, J. Frey, J. Cramer

This past year saw the completion of the Cooler ring construction phase. As a result of a lot of hard work by the members of the installation crews, all basic ring components (magnetic elements, vacuum enclosures, rf cavity, beam diagnostic elements), along with their associated services (power, cooling) and controls, were essentially in place and operating by the end of October 1987, with the exception of the electron cooling system and the internal gas jet target systems which came on-line by the end of March 1988. Figure A1 shows a schematic view of the completed ring.

The ring dipole magnets, having been installed and powered up by the end of 1986, were undergoing ramping tests in the first quarter of 1987. The main assembly task in the spring and summer quarters was the installation and alignment of most of the 36 ring quadrupole magnets (at the rate of one pair of quads per week) and the 18 hexapole magnets.

By the end of June 1987, all 28 of the ring quadrupoles (and 16 of the hexapoles) outside of the cooling region were in place, along with their vacuum chambers. Installation of the remaining 8 quadrupoles in the cooling straight section could not proceed until in-place field mapping of the electron confinement solenoid was completed. Quadrupole installation proved to be an exacting and hence slow task, involving an intricate sequence of assembly steps. This included installation of the vacuum chamber subassemblies, with tight tolerances on the location of the integral beam position pickups, within the aligned quadrupole gaps. Preparation of the quad chamber subassemblies, after initial welding in our shops, included a commercial high-temperature vacuum oven bake, then final welding with hexapoles and beam position pickups in place, followed by addition of heaters and thermal insulation.

Work on the electron cooling system magnets proceeded in parallel with ring construction during this period. After delivery at the end of March of the 3 solenoids, some minor mechanical modifications to the support mandrels, and the addition of locally-produced dipole steering coils and correction windings at the junctions between solenoids and toroids, the system was assembled and services were connected in preparation for field mapping during the summer.

Work in July concentrated on the completion of the injection region in preparation for first beam injection into the ring on July 30. The last quadrupole doublet of the injection line was put in place, followed by installation and alignment of a set of 10 small dipoles associated with injection (Lambertson septum magnets and other unconventional magnetic elements) together with intricate welded vacuum chambers for threading the beam through this three-dimensional maze to the midpoint of the injection straight section of the ring.

Also during July the balance of the overhead shielding beams was delivered, stacking

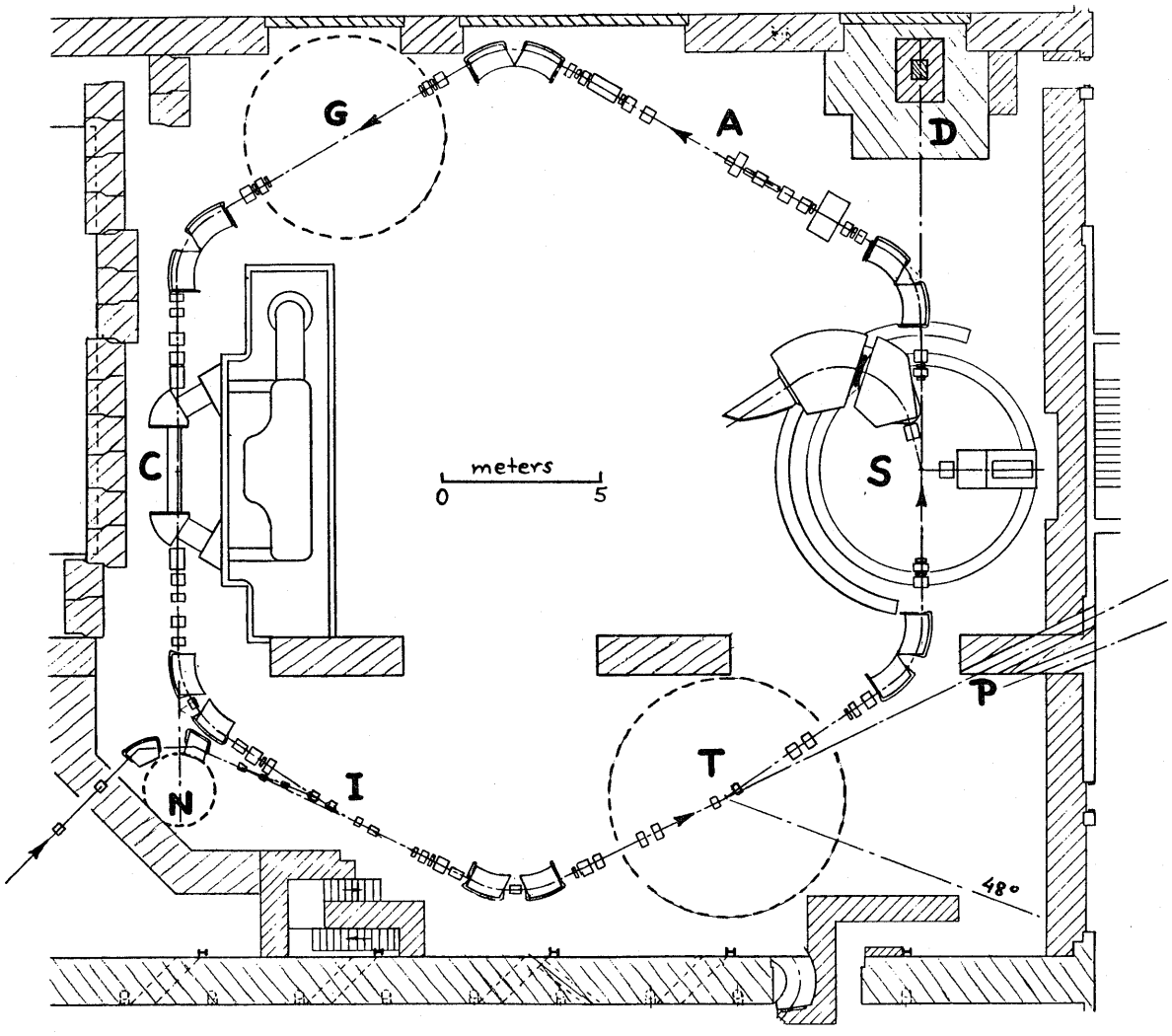

Figure A1. Schematic layout of the IUCF Cooler storage ring. Key to labeling: I - injection straight section, T - tagged secondary beam production region, P - 0° time-of-flight penetrations, S - spectrometer section (with future spectrometers sketched in), D - beam dump for 1/3 turn, one-pass experiments, A - acceleration and rf manipulation straight-section (with space for target facility), G - general-purpose target region (now occupied by gas-jet target and CE-01 detector array), C - beam cooling section with electron gun and collector HV terminal, N - neutral particle detection area (for H° atomic physics experiments).

of concrete-block mazes was completed, and lights were installed below the roof shielding level.

The goal for the rest of the summer quarter was to complete enough of the ring to carry the beam through 2/3 of the circumference in tests scheduled for September. This entailed installing and vacuum testing a number of main dipole vacuum chambers and straight-section vacuum pipes as well as installation of a number of small steering dipoles in that portion of the ring.

On September 30, the beam was successfully carried through 2/3 of the ring. To reach that point required a few temporary hookups, and hence the installation workload for the month of October included not only completion of the last 1/3 of the ring but also cleanup of a number of loose ends generated by the hectic pace of the August installation period and the September test run support period.

The winter quarter 1987 marked the terminal phase of ring assembly and first operation of the IUCF Cooler as a storage ring. Construction periods alternated with beam testing periods. These beam tests are described in the next section. During the 4-week construction period in October, installation of the 8 quadrupoles and the 6 strong steerers in the cooling straight section was accomplished and the first complete ring vacuum attained (though with a temporary beam pipe in the cooling section). During the mid-November to mid-December construction period, an intense effort by the controls hardware group was made to prepare most of the ring elements for ramping. The first of two ferrite kickers for non-stripping injection was installed. The vacuum in the injection line was improved by repairing small leaks and bringing some cryopumps into service. This, coupled with partial bakeout of ring vacuum chambers, resulted in the necessary improvement in average ring vacuum to the 10^{-8} Torr level consistent with reasonable lifetime of stored beam. The ferrite-tuned rf system was operated with good vacuum in the beam tube and showed no problem with control under multipactoring. In late December the toroids and solenoids of the electron confinement system, along with its family of compensating steerers and solenoids, and most of the ring hexapoles were activated for the first time with beam in the ring.

The intense effort to complete the ring vacuum enclosures in preparation for beam storage tests created delays in completion of the electron system. It was not until November, after the ring began operation in storage mode, that fabrication of the gun and collector subassemblies and the long cooling-region vacuum chamber could be finished. Several other major hardware components fabricated outside were also very late in arriving.

Assembly of the electron cooling system took place in the first quarter of 1988. After the last of a set of small but very troublesome leaks in the long solenoid vacuum chamber was repaired, this complex subassembly was baked repeatedly to verify that temperature cycling would not open up new leaks. In parallel with this, the gun and collector subassemblies were being assembled and baked. Breakage problems encountered with the insulating rods which keep the cantilevered high-voltage accelerating tube in compression necessitated some redesign. When the long vacuum chamber had proven vacuum tight it was installed within the long solenoid, the gun and collector assemblies were mated to it, and the entire system baked once again. Sealing problems with some (at this point barely accessible) flanges had to be solved before a leaktight system was obtained. Thus

the decision made early in the project to assemble the electron system off-line on a rolling platform near the final location proved its value in separating the ring and electron system vacuum problems until the last moment.

The electron system came into operation in its off-line test position on March 30 and behaved extremely well from the start, generating a 1A electron beam at 125 keV with 99.94% collection efficiency within a few hours of first turn-on. This smooth start-up after strenuous and often hectic effort to assemble this intricate system on a tight time schedule is a direct consequence of the careful attention to detail by its designers. The electron system was finally rolled in place as an integral part of the IUCF Cooler ring in early April 1988, and electron cooling of a proton beam was first observed on April 16.

The first quarter of 1988 also saw the installation of an internal target system in the Cooler ring. After assembly, alignment and testing of the gas jet target facility in its off-line location during January and February 1988, this structure was moved into position in the "G" straight section of the ring and aligned during a 3-week interval between Cooler ring test runs in late February/early March. On-line tests demonstrated vacuum integrity and the effectiveness of the differential pumping system in maintaining good ring vacuum away from the target region with gas jet operating. First observation of scattering events of stored beam from the internal jet target, and of the effect of the target gas on beam lifetime, was made on March 10, and studies of the interaction of a cooled beam with this target were initiated on April 17.

A.3. Cooler Commissioning, R. Pollock, T. Ellison, D. Friesel, P. Schwandt, W. P. Jones, T. Rinckel, T. Sloan

Beam runs for Cooler testing commenced October 30. In the 6 months following, beam testing periods of about 4 days duration, typically every 2-3 weeks, on the average, alternated with construction periods.

The winter quarter marked the first operation of the IUCF Cooler as a storage ring. Test runs during this period yielded significant data for understanding the basic ring characteristics. The spring 1988 quarter marked the first operation of the Cooler as a synchrotron accelerator, as an internal target scattering facility, and finally as an electron-cooled beam storage ring. Test runs during this period also yielded substantial improvements in operation as a storage ring, with significant increases in stored beam intensity (up to 10^9 protons, or about 0.15 μA) and in storage lifetime (mean life $\tau_{1/e}$ up to 4 sec uncooled and up to 45 sec cooled, at 45 MeV).

A.3.1. Highlights of Cooler Operation

- July 30-31; August 5: beam injection into ring. Tests of injection hardware, verification of injection beam line optics.
- September 11, 17: stripping injection (90 MeV $H_2^+ \rightarrow$ 45 MeV p+p); beam transported halfway around ring. Preliminary dipole and quadrupole perturbation surveys to check ring optics and identify setting errors.
- September 29, 30: 45 MeV proton beams transported through 2/3 of the ring. Ring surveys repeated.

- October 30, 31: beam carried around one complete turn.
- November 2, 3: multiple turns observed. Orbit frequency measured, cyclotron energy changed (at constant frequency) for better match to ring momentum acceptance. Ring rf system excited to trap injected particles into phase-stable orbits.
- November 6: first longitudinal Schottky signal indicates 90 turns with circulating current of 3 μA; synchrotron sidebands observed.
- November 7: change from continuous to intermittent injection using "beam splitter" kicker magnet in beam line from cyclotron, allowing direct observation of decay lifetime of stored beam.
- November 8: turn number raised to 200. Measured and minimized closed-orbit distortions of stored beam. Observed weak, long-lived tail on beam; optimization of its intensity yielded record mean life of 9,000 turns, permitting first betatron tune measurements by gated horizontal and vertical rf knockout, and observation of transverse Schottky signals.
- December 18-20: systematic ring survey of single-turn beam shows partial agreement with expected phase advance (much better than in Nov.). Aperture function surveys and betatron tune measurements made. Synchrotron motion of beam captured into ring rf bucket showed increased momentum acceptance with improved tune.
- December 21, 22: exciting the fast turnoff injection bumper magnets raised mean lifetime to 150 ms from the 10 ms maximum lifetime observed up to now (consistent with limits imposed by stored beam passing through stripping foil).
- December 23: long-lived beam observed with toroids and solenoids of electron confinement system excited (after closed orbit corrected with compensating steerers).
- December 28-31: studied effects of ring vacuum perturbation and ring aperture restrictions on beam lifetime; achieved vacuum-limited mean lifetime of 0.34 s at 50 nanoTorr average ring vacuum. Measured ring momentum acceptance and surveyed dispersion around ring.

1989 ↓

- January 21, 1988: after improvements in average ring vacuum to about 25 nanoTorr, observe mean lifetimes up to 1.4 s. Reduced vertical dispersion in ring by a factor of two using a skew quad.
- February 15: first successful execution of fill-store-accelerate-store cycle with modest energy ramp (from 45 to 65 MeV in 0.5 s). Mean lifetime of 2.4 s at 9 nanoTorr average ring vacuum.
- March 10: internal gas jet target operating (CW mode) with stored beam; first scattering events from N_2 jet observed with scintillation detector array covering the forward cone $1.5° < \theta < 10°$.
- March 19-21: acceleration from 45 to 148 MeV on a 1.7 s ramp; stored beam at 148 MeV with 3×10^7 protons and lifetime in excess of 10 s. Mean lifetime of 3.6 s achieved at 6 nanoTorr average ring vacuum for 45 MeV beam. Beam lifetime measurements and scattering data taken at 45 MeV for H_2, N_2, Ar target (typical values: 10 nanogram/cm^2 N_2 thickness, luminosity $\sim 5\times10^{28}$ cm^{-2}sec^{-1}, $\tau_{1/e} \sim 1$ s). First attempt to take data at 148 MeV.

- March 30: first off-line operation of complete electron beam system at 50-125 kV and currents up to 1A with typical losses in the 2-5$\times 10^{-4}$ range.
- April 2, 3: exploration of horizontal and vertical tune space for best lifetime with chromaticity correcting hexapoles on and off.
- April 4: accelerated and stored again at 148 MeV; scattering measurements at 148 MeV with pulsed gas jet (0.2 s turnon/turnoff time constant).
- April 5, 6: successfully injected 90 MeV deuteron beam into ring through "stacking injection" path, but intensity too low to search for stored beam.
- April 16: achieved first electron-cooled 45 MeV proton beam; observed order-of-magnitude increase in mean lifetime (up to 43 s) and reduction in beam energy spread (from 50 keV to 3.5 keV FWHM). Measured longitudinal drag force and cooling time.
- April 17: first cooled beam on internal H_2, N_2 target; measured lifetime vs. target density in agreement with expectations.
- April 24-26: systematic cooled beam studies with and without target; observe $\Delta p/p \sim 2 \times 10^{-5}$ (FWHM). Accelerate cooled 45 MeV beam to 148 MeV.

A.3.2. Beam Injection

Essentially all Cooler testing through April 1988 has been carried out with 45 MeV protons accumulated in the ring by the stripping injection of 90 MeV H_2^+ ions from the cyclotron, using a 20 μg/cm^2 carbon foil stripper. The ring is filled while the closed orbit is locally perturbed upward, using a set of 3 fast-turnoff "bumper" magnets, to pass through the foil stripper and to coincide with the incident beam path. When the magnets producing this transient bump in the orbit are switched off, the beam path is deflected by constant steerers producing a static bump of opposite sign that holds the beam path below the stripper foil for storage.

The cyclotron routinely delivers H_2^+ currents of 0.3-0.5 μA for Cooler injection. To fill the ring, a short beam pulse of 5-10 ms duration is diverted down the Cooler injection line by a switchyard splitter magnet, with timing and repetition rate selected by the Cooler operator. At 0.5 μA, a 5 ms pulse of H_2^+ after stripping is expected to deliver about 3×10^{10} protons into the ring. We observe typically 70% of the expected proton flux at the first beam stop within the ring, the loss attributed to injection inefficiency. The largest stored current we have obtained in the ring is 10^9 particles, about 0.2 mA or 5% of the protons in principle available after injection. The cause of this accumulation inefficiency has not been located. We can tune the orbit while the beam is passing through the stripping foil to obtain a lifetime of order 3 ms, or 3×10^3 times the orbit period. Accumulation for this time should give 10^{10} particles stored rather than the 10^9 observed. The time dependence of the decay during filling appears to still contain a second, shorter-lived component which may be indicative of a phase-space shape mismatch between ring and incident beam. We have deferred a detailed investigation of the loss mechanism during filling for now as stored beams of 10^7-10^8 particles are sufficient for ring development activities. However, the higher currents are essential for the high luminosities planned for most of the experimental program.

Of more immediate concern is the intense burst of radiation produced as excess beam is lost during the brief period while filling is in progress. This is a considerable nuisance to operation of detectors in the ring, requiring wire chamber HV biases to be gated off during the fill period on each cycle, for example. We need to understand the loss mechanism in order to control the azimuthal distribution of losses around the ring so they are never seen at the locations of sensitive detectors.

There is also a brief beam spill when stored beam remaining in the ring is dumped prior to refill: because bumper rise times are not well enough matched, the beam develops a large vertical closed-orbit distortion as the bumpers turn on. This loss, we found, can be minimized in the target/detector region by adjusting the shape of the closed orbit so that this beam loss occurs elsewhere in the ring.

A.3.3. Beam Storage

Multiturn beam accumulation in the ring is accomplished in a series of well-defined steps. Using the beam position monitoring (BPM) system described in a later section, the dipole fields are easily adjusted to produce a well-centered single-turn orbit. With the ring quadrupoles correctly set (based on ring lattice calculations, modified by results of experimental aperture function and tune surveys), some beam begins to accumulate with tuning of the injection matching conditions. The stored current read on BPMs, sampled during the brief (5 ms) interval when the bumper and splitter magnets are on, is a good indicator of the accumulation factor and is maximized to reduce closed orbit distortions and to optimize the match of the injection line to the ring, as shown in Fig. A2. The ring rf cavity must be excited to maintain the high-frequency modulation of intensity to which the

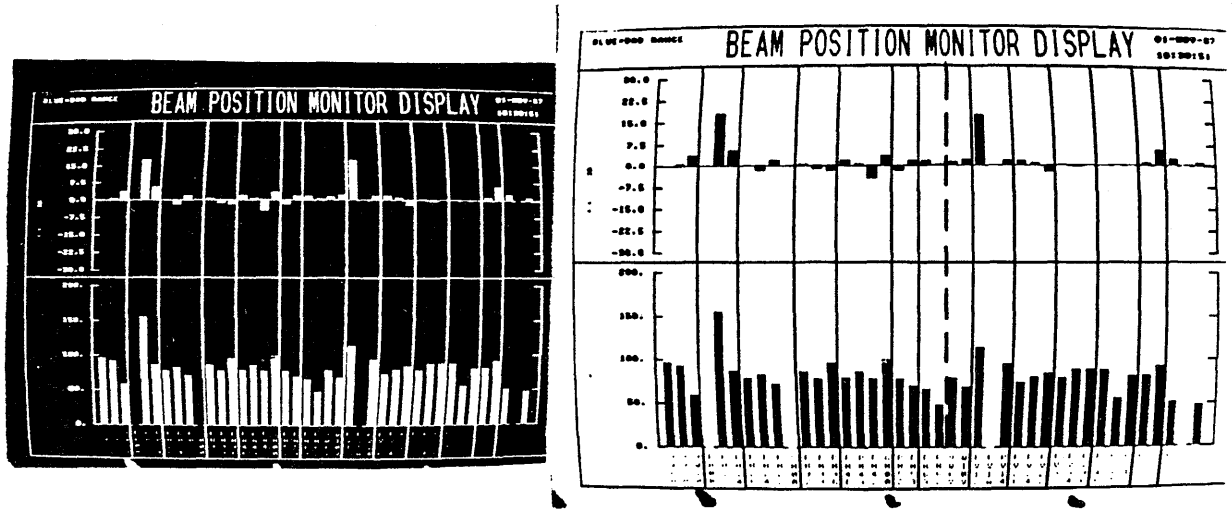

Figure A2. Beam Position Monitor display. The horizontal (vertical) beam position (± 30 mm) and intensity (200 nA) are displayed on the left (right) side of the screen. The first 3 (2) monitors are in the injection line. A beam loss towards the end of the ring, as well as the beginning of a second turn towards the beginning of the ring, is observed.

BPMs respond. Suitably synchronized displays of wall-gap monitor signals then also show the synchrotron oscillation pattern and the time development of the longitudinal phase space area arising from repetitive passage through the foil stripper. When the stored current indicates accumulation of the order of 10^2 turns, the operator begins to search for a long-lived component of the beam surviving after the injection bumper and splitter magnets have turned off. Stored beam lifetime can then be increased from of order 10 ms to several seconds by fine tuning of the injection matching and bumper magnets, ring main dipoles, horizontal and vertical quad tune combos (see below), and ring rf phase.

The lifetime of stored, uncooled beams of 45 MeV protons increased markedly during the first few months of operation with improvements in the average ring vacuum as a result of outgassing of laminated injection magnets and ferrite kickers, bakeout of an increasing fraction of the ring vacuum enclosures, addition of pumps and repairs of small leaks. Between mid-December 1987 and mid-February 1988, as the average residual gas pressure in the ring fell from 150 to 10 nanoTorr, the mean lifetime increased from 0.2 to 2.4 s. Average pressures as low a 5 nanoTorr were measured in the March and April 1988 runs; a complete ring bakeout should give about 1 nanoTorr.

Beam lifetimes of several seconds, together with the ability to refill the ring every few seconds, allow the use of various diagnostic procedures and are quite adequate for systematic studies of ring parameters and ring operation in fixed-energy storage mode; it permits energy ramping and beam measurements after ramping to be carried out as well.

The techniques used for many of the measurements of transverse and longitudinal phase space properties of the stored beams, along with sample results, are described in a later section of this report entitled "Beam Diagnostic Systems". Here we shall discuss only two principal stored-beam characteristics, betatron tune and energy dispersion, in some detail.

In early test runs a stable ring tune was found empirically, with quadrupole currents somewhat different from lattice predictions. Searches for quad faults (interconnect errors, coil shorts, etc.) produced none. It appears that the extreme sensitivity of the ring tune to the edge angles of the corner dipoles is responsible. Treating those edge angles as free parameters, agreement with measured tunes was found by setting the outer edge angles of a dipole pair 0.6° away from the mechanical angle (in the vertically focussing sense), in accord with dipole field maps, while setting the interior angle equal to the mechanical angle. This is not unreasonable since the interior edges of a dipole pair are close together and truncation of the fringe field in the overlap region may drastically reduce the 0.6° rotation present for an isolated edge. This effect raises the horizontal tune enough to put the ring into the Q_h=9/2 stop band if not corrected by changes in quadrupole strength. The quad absolute strength is also scaled down by 0.8% in obtaining agreement between predicted and measured tunes.

Horizontal and vertical tune combinations have been constructed by coupling together (via control software) groups of appropriate quads in linear combinations (with relative strength coefficients derived from lattice design). These combos allow large displacements in tune space while the beam is stored. We can, for example, move the tune to sit exactly on the Q_h=17/4 resonance and observe a reduction of a factor of 2 in lifetime. This is a test of the strength of octupole errors in the lattice elements. Or we can move

the beam to Q_h=13/3, where the lifetime is short, and adjust hexapoles in non-dispersed regions to recover a reasonable lifetime. Trying to repeat this trick at Q_v=16/3 has not yet succeeded, although we did accelerate the beam across this resonance line inadvertently on our first energy ramp to 148 MeV, losing an order of magnitude in intensity in the process.

The most stable region in tune space appears to lie in the vicinity of Q_h=4.29, Q_v=5.18. More systematic explorations need to be done, however, to identify those resonance lines (out of many possibilities) which significantly affect lifetime. Cooled beams, with their greatly reduced tune spread, will be an incisive tool in future studies of this kind.

We will also have to devote more running time to detailed verification of the ring lattice parameters. This is essential data for the calibration of local orbit correction combos (dipole or quad control variable combinations) and for other operational improvements, such as automation of many lattice or orbit control operations, and aperture maximization.

One of the remaining mysteries in the storage ring operation is that we appear to obtain better lifetimes (larger acceptances) when operating the ring with non-zero closed orbit distortions, i.e., with beam deliberately offset from the axis defined by the BPMs by several millimeters, in some cases. Until recently, uncertainties in the lattice parameters have delayed the development of the family of localized orbit perturbations that will allow us to track down the source of this behavior.

By the end of the spring 1988 quarter, we had control of all ring hexapoles and had some modest initial success in using them to reduce chromaticity and increase beam lifetime. The rf knockout resonance used to measure the ring tune was also observed to become much sharper at reduced chromaticity. In order to set hexapoles in the non-dispersed regions, however, we still need to develop a way to measure the increase in off-momentum transverse ring acceptance. The closed-orbit distortions mentioned above also complicate hexapole explorations because each hexapole is both a steerer and a lens for off-axis beams.

The dispersion function of the ring was measured by energy modulation of the stored beam. Once the beam is stably confined within an rf bucket, its energy can be changed by sweeping the rf frequency. At sufficiently large beam intensity ($\sim$ 1 μA) and lifetime, the BPM system has enough sensitivity and bandwidth to follow position changes over several complete energy cycles as a triangular wave modulation (of 0.1% peak-to-peak at 10 Hz) is applied to the rf frequency and hence to the beam velocity. Such a measurement is shown in Fig. A3. By looking at BPM pickups around the ring in this mode, we were able to establish that the dispersion is large (about 4 m) in the three straight sections where it is supposed to be 4.2 m, and small (<0.5 m) elsewhere. The technique is sensitive enough to show that the dispersion is not exactly zero where it is supposed to be zero. In particular, we observed the dispersion to deviate significantly from zero in the vertical plane. The vertical dispersion persisted when the electron-confinement solenoids (which can couple horizontal and vertical phase space) were turned off. Analysis of this problem traced its source to a skew quadrupole error field near the injection point. Indeed, field maps of the injection septum magnet showed fringe-field error terms of the right magnitude to explain the data. A single skew quadrupole magnet was subsequently added to partially correct for this field error and in fact reduced the largest vertical dispersion by a factor of

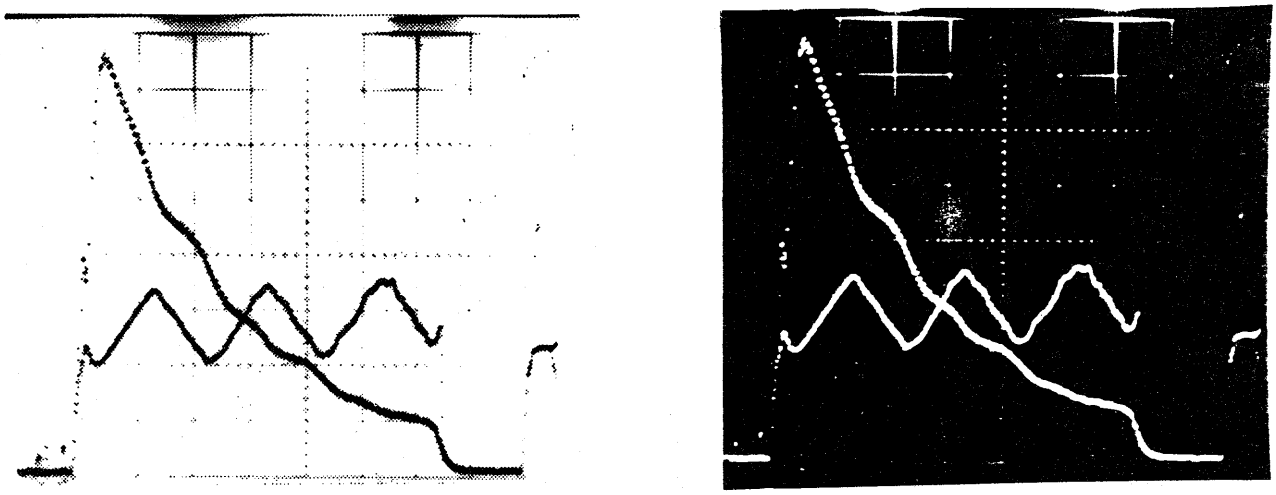

Figure A3. Beam dispersion measurement. The triangular waveform is the beam position signal and the exponentially decaying waveform is the beam intensity signal, both from the BPM system.

two.

In summary, we clearly have a working storage ring. With stripping injection, beam intensities and lifetimes are large enough to allow development of other Cooler functions, such as acceleration, electron cooling, and first experiments with internal targets. Surveys have shown that much of the ring has the design optics (with persistent disagreement in some details). Our ability to measure phase advance, aperture and dispersion functions, and betatron tunes allows us to improve ring performance, optimize parameters and track down remaining problems. Many non-trivial procedures are under control: matching the injection cyclotron to the ring; establishing a closed orbit concident with the injection path; synchronous capture into the ring rf buckets; applying local corrections to thread the beam through the very large dipole perturbations of the electron-confinement region (which exceed the ring acceptance many fold) without losing the closed orbit.

A.3.4. Beam Acceleration

Acceleration of a stored, uncooled 45 MeV protons to 65 MeV occured on February 15, 1988 and to 148.4 MeV on March 20. These first successes in energy ramping represent a significant verification of the hardware/software control concept underlying operation of the Cooler ring as a synchrotron. The people (particularly T. Bertuccio, W. Manwaring, J.Collins) who delivered so much working logic hardware and its associated complex computer code for ramping over 70 ring magnet and rf cavity supplies, and ran shifts with us to help debug on-line, deserve much credit for delivering under pressure.

The "ramp cycle" when operating the Cooler in synchrotron mode consists of a freely-chosen time at the higher energy during which an experiment may be performed, followed by a sequence of events: the "reset" interval, in which the energy in the dipole field is

dumped with an L/R decay time of 2 s, and all elements are brought to a magnetic field level below the injection level; a "ramp-to-fill" interval, in which all magnets are brought back to the values which gave stored beam at the injection energy; a "ramp-to-run" interval, in which the acceleration takes place; followed by the next cycle of the experiment, with beam stored at the higher energy.

The first step in ramping is to calculate from the existing state of the machine how each element should change as the energy is raised, taking account of non-linearities. The calculation is performed in a few seconds by our control computer and generates a slope-endpoint data table for each power supply, which may then be downloaded into a ramp control card for that supply. The non-linear ramps are executed by these cards when a "ramp start" command is issued. When ramping is stopped, the cycle ends at the "fill" level so operation in storage mode at the injection energy can be checked. If stored beam performance has deteriorated after the ramp because of the altered hysteresis cycle, the ring is simply retuned, the calculation repeated starting from the improved settings and the ramping resumed. This iterative process may be repeated as often as necessary until the performance after the ramp ends is indistinguishable form the initial state.

First trials of this procedure were fairly disheartening, as a nicely-tuned ring would be replaced after a ramp cycle by a black box with no trace of beam. As bugs were removed (quads ramping to full scale, etc.) and our setup procedures improved (taking critical elements such as the ring main dipoles through an approximation of the desired hysteresis cycle before calculating the ramp), the situation improved. Our first demonstration that the process converges occurred on January 30, when beam was observed storing at the fill level during each ramp cycle. The beam totally disappeared as soon as the ramp began, but at least it existed!

Cooler ramps take place at constant dp/dt. The design value of this slope is 1 Tesla-meter/s, so that 2.6 seconds will be sufficient to take a beam from the stripping injection rigidity of 0.98 T-m to the 3.6 T-m ring rigidity limit (45 MeV to 495 MeV for protons). In our tests to date, we have used ramp slopes of about 0.5 T-m/s, to reduce the overvoltage demands on the dipole power supply.

The beginning and end of the constant $d(B\rho)/dt$ region of the ramp require special treatment. Some of the ring elements have finite risetime. For example, the hexapoles are not laminated, and their field lags the current by 13 ms. The main dipole supply has an output ripple filter, and even when special vectors are added to the slope-endpoint tables for this element, to smooth the transient response, about 60 to 70 ms are needed to bring the slope up to full value. Other elements then have their ramps in this transition region shaped to conform to the dipole. The program has parameters which can be adjusted while comparing inductive voltage pickups in a representative dipole and quadrupole. The sensitivity of matching is such that differences must be undetectable to the eye for the beam to accelerate. The half-speed ramps used in first acceleration trials also slightly ease the stringency of the required match.

In the February runs, there were a number of residual software bugs which were not preventing acceleration, but were slowing our progress. An example is a dipole mismatched to the desired rigidity, arising from the complexity of the transient suppression scheme. Acceleration in the February 9-15 run was accomplished by interactive adjustment of

ramp waveforms to gradually uncover this and other mismatches, providing feedback for improving the calculation. The interactive mechanism at this time was still relatively primitive, requiring direct substitution of hand-calculated entries in selected slope-endpoint tables. By February 11, we were halfway through the ramp by adjusting the rf frequency to compensate for the dipole error, and by February 12 had reached the region of the ramp end transients. Fine adjustments showed that beam losses during acceleration could be reduced to 10 or 20%.

After some digressions, the study of acceleration resumed on February 14 and in the early hours of February 15 the beam was observed to store after the ramp had ended and the turnoff transients had died away. This was a modest change of energy, from 45 to 65 MeV in 0.5 s, but a welcome demonstration that we could control the basic fill-store-accelerate-store cycle on which our research plans depend.

Acceleration studies resumed on March 10, on a 1.7 s ramp to 148 MeV (both of the first two ramp energies were chosen to match the needs of early approved experiments). The dipole calculation and the user-friendliness of the interactive ramp correction was much improved by this time, so progress in developing the higher energy ramp was rapid, and beam was observed accelerating for about 0.7 s (to about 72 MeV) a few hours later as this short run ended.

Ramping to 148 MeV resumed on March 19, after a tune space exploration to select a tolerant working point. Within about two shifts we had a trace of beam near the end of the ramp and had measured tunes during acceleration, which were changing significantly (even crossing the Q_v=16/3 resonance) and required quad strength modifications (a calculational error, corrected for the April runs). The match between rf frequency and main dipole field required only smooth adjustment of about 0.4% to reach the end of the ramp. Stored beam at 148.4 MeV was achieved, at an intensity of about 3×10^7 stored protons and lifetime in excess of 10 seconds at this higher energy. Acceleration and storage at 148 MeV was repeated on April 4, and scattering measurements with a pulsed gas jet target and a study of target thickness-lifetime relationship were carried out at this higher energy.

On April 26 we accelerated for the first time an electron cooled 45 MeV beam beam to 148 MeV. Cooling prior to acceleration clearly makes ramping considerably easier; the process is more tolerant of remaining slight ramp start errors and minor ramp waveform mismatches. The acceleration of cooled beam, however, places unusual demands on the ramping controls because the electron confinement fields stay constant, and some steerers governing higher-order orbit corrections have their strengths decreased with time during the ramp-to-run interval.

A.3.5. Beam Cooling

After successfully commissioning the electron cooling system off-line on March 30 of this year and installing it in the ring a week later, the first cooling of a stored 45 MeV proton beam was attempted on April 15.

Using the BPMs installed at the gun and collector ends of the long confinement solenoid to measure both proton and electron beam positions (the latter by modulating one of the gun anodes by 10V at 1 MHz, thus modulating the electron beam intensity by $\sim$ 10 μA), we were able to overlap and align the two beams to within 10% of the

electron beam diameter (2.5 cm) in relative position and to within 1 mrad in relative angle. Immediately after achieving beam alignment and beam velocity matching (by fine-tuning the electron beam energy) in the late hours of April 16, proton beam cooling was observed with the greatest of ease by watching (a) the peak width of the Schottky signal frequency spectrum (proportional to momentum spread) narrow sharply and rapidly (within ~1 sec), (b) the time spread of the rf-bunched beam, as displayed by a wall-gap monitor signal, reduce sharply, and (c) the lifetime of the stored beam increase dramatically (by an order of magnitude). Figure A4 shows a Schottky signal from this first observation of beam cooling.

A series of measurements of longitudinal and transverse cooling rates and of the equilibrium beam properties were made on the 45 MeV cooled beam during this run and on a subsequent run during the April 24-26 period when cooled beam studies with a pulsed gas jet target operating in the ring were also carried out. Preliminary results from these recent investigations are presented in the next section.

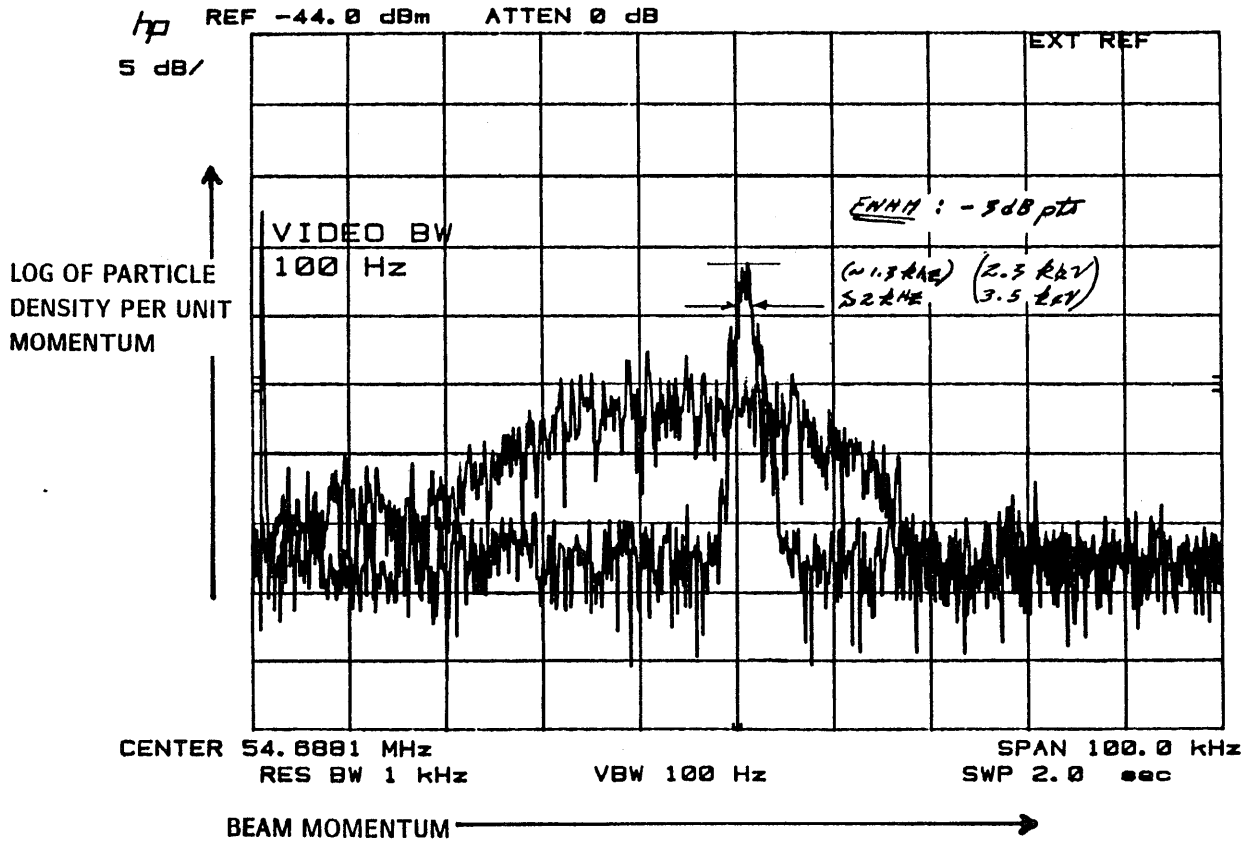

Figure A4. First observed cooling of a 45 MeV proton beam with a 0.3 A electron beam. Injected $\Delta p/p \sim 0.08\%$; cooled $\Delta p/p \sim 0.003\%$.

A.4. The Electron Cooling System, T. Ellison, D. Friesel, B. Brown, O. Dermois, J. Self, and B. Starks

The electron cooling system was commissioned March 30, 1988. During the first evening of operation, the system smoothly generated a 1 A electron beam at 125 keV (the design limit without the use of SF_6) with collection (electron recovery) efficiencies of between 99.9% and 99.99%. In later operation, collection efficiencies as high as 99.995% have been observed. The electron system was subsequently installed in the ring. On April 16, 1988 the first cooling of 45 MeV proton beams was performed and equilibrium proton beam energy spreads of 2-3 keV were observed. Since then, the Cooler has been in routine operation. Subsequent measurements of the cooled beam emittance indicate that the proton beam temperature in the cooling region is within a few times that of the electron cathode temperature.

Below, measurements of the electron cooling system magnetic fields, and preliminary measurements of the cooling system performance are summarized.

A.4.1. Introduction

The electron cooling system produces an intense electron beam with a very low rest frame temperature. Table I lists some of the design and measured parameters of the electron system, and Fig. A5 shows an overview of the system as it is presently installed in the Cooler ring. In the cooling section of the Cooler storage ring the ion beam closed orbit is made to precisely match the trajectory of the electron beam. If the average velocity of the ion beam is close to that of the electron beam, the two beams strongly interact, and the ion beam is cooled to an equilibrium temperature very close to that of the electrons. The cooling takes on the order of 1 second. The cooled ion beam has extremely good energy and spatial resolution: ΔT (FWHM) $\sim$ 2 keV, Δx (FWHM) $\sim$ 0.5 mm.

Table I. Electron Cooling System Design Parameters

Electron Beam Energy	7-275 keV (5-125)*
Electron Beam Current	0-4 A (0-1)
Electron Beam Diameter	2.54 cm
Electron Gun Perveance	0.7×10^{-6} A/V$^{3/2}$
Transverse Electron Beam Temperature	0.1 - 0.2 eV
Electron Gun Accelerator Column Length	62.3 cm
Max. Column Electric Field Gradient	11.3 kV/cm
Nominal Solenoidal Magnetic Field	1.5 kG
$B_\perp/B_\parallel$ in the Cooling Solenoid	$< 0.5 \times 10^{-3}$ (1×10^{-4})
Effective Cooling Region Length	270 cm (230)
Collector Efficiency	>99.9% (99.9-99.995%)

*The values in parenthesis are measured values

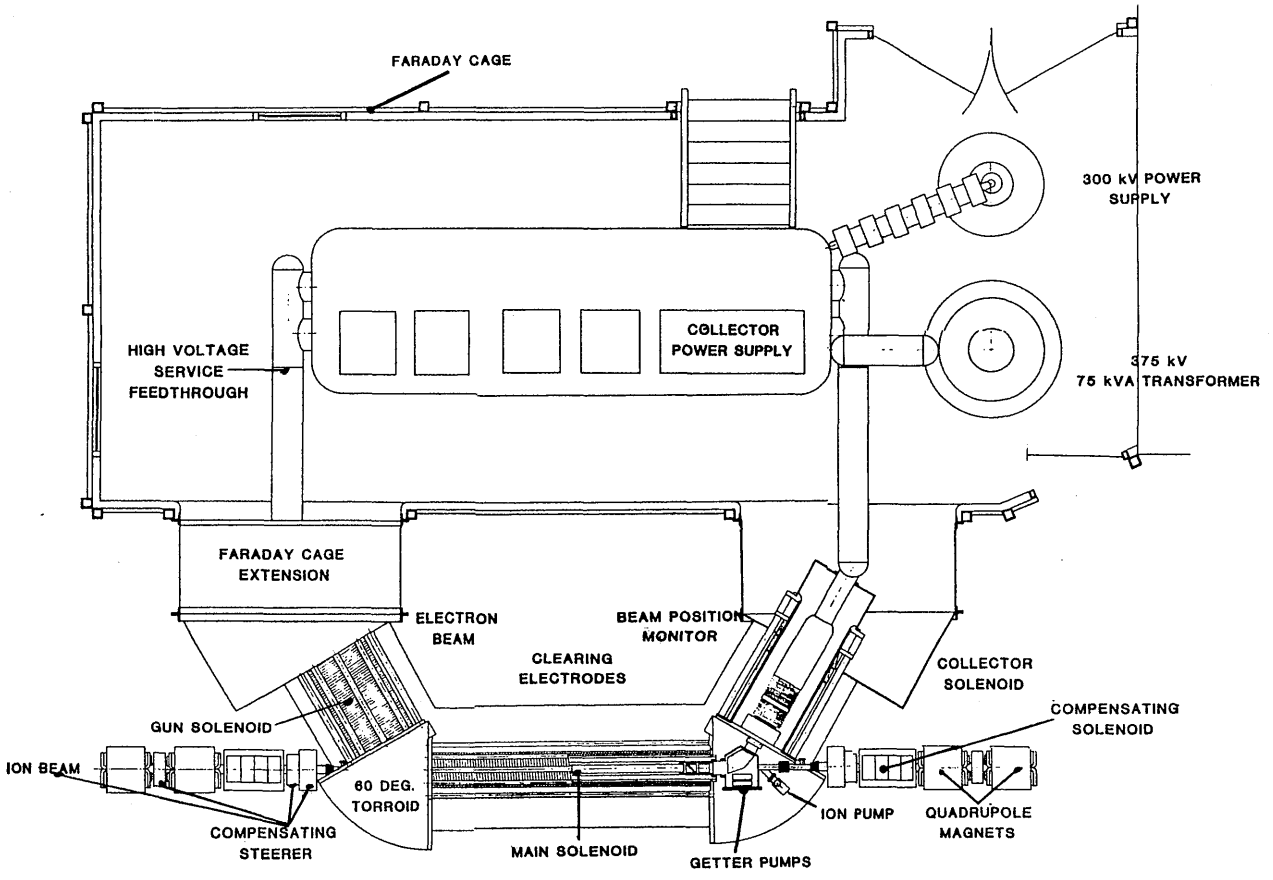

Figure A5. Top view of electron cooling system installed in ring. (The main solenoid is 3 m in length).

A.4.2. Magnetic Field Measurements and Corrections

The electron beam magnetic guide field must be constructed such that it does not induce effective temperatures in the electron beam. Throughout the system the electron beam is confined by a longitudinal solenoidal field. Ideally, the electrons should adiabatically follow these field lines which should be perfectly straight inside the main 3 m length solenoid where the cooling takes place. One important form of "heating" is the existence of transverse fields in the cooling solenoid which cause the electron beam to adiabatically move with an effective transverse momentum. Figure A6 shows the measured transverse field components in the main solenoid before and after correction. The effective transverse energy due to the rms angular deviation of the corrected field lines varies from about 2.5×10^{-4} to 3.5×10^{-3} eV as the electron beam kinetic energy varies from 20-270 kV. This should be compared with the cathode temperature which is about 0.2 eV.

Another source of effective heating is field errors which lead to nonadiabatic motion of the electrons, or to a coherent oscillation of the electrons about the field lines. In the IUCF electron cooling system there are large longitudinal field strength errors where the

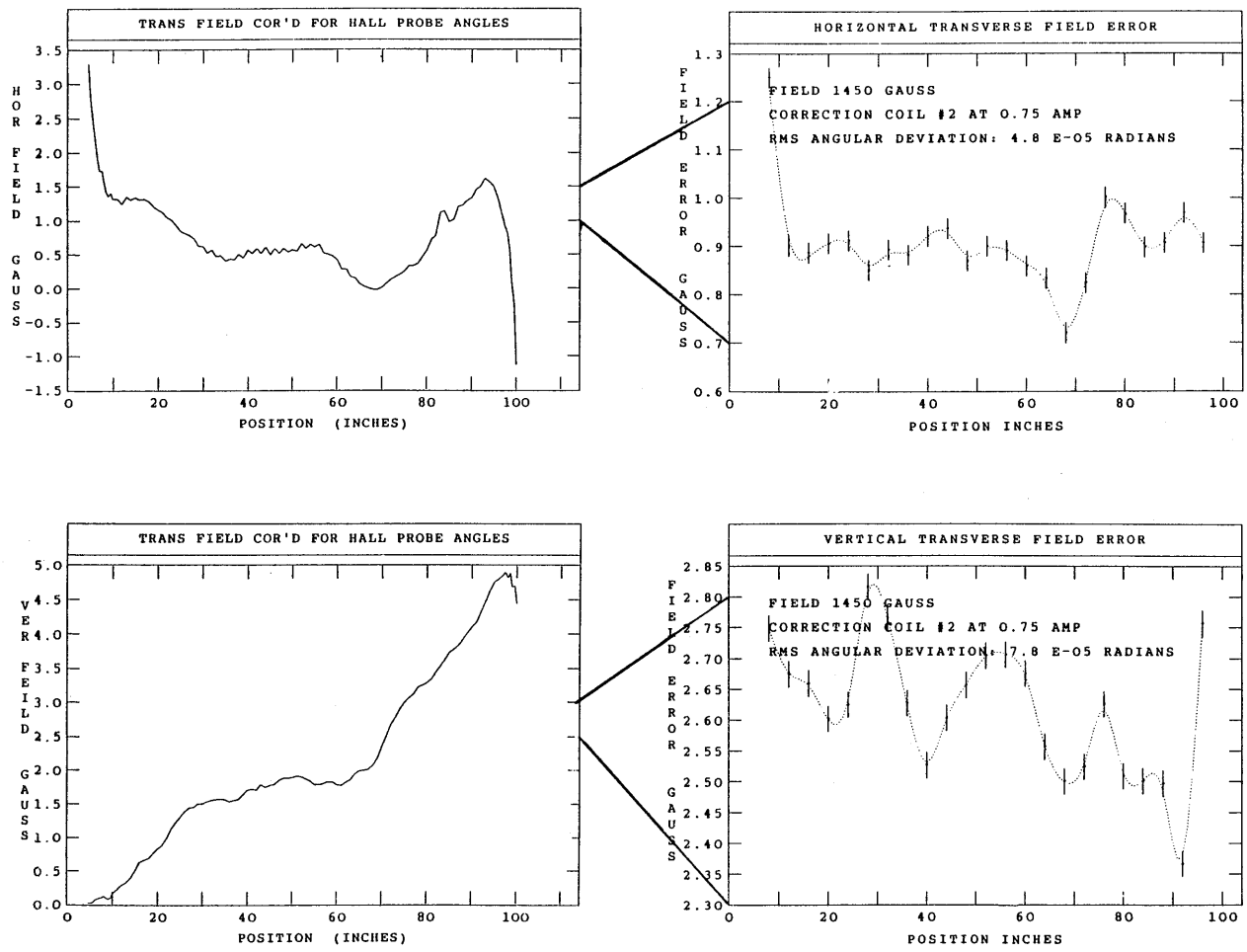

Figure A6. Measured transverse fields in main 3 m cooling solenoid before and after correction.

solenoids join to the toroids. These errors, as shown in Fig. A7a, are due to the absence of current carrying conductor at these locations. To study the effect of these perturbations a simple particle tracking program was written. The results were surprising at first glance, showing that the first order corrected fields, as shown in Fig. A7b for example, lead to higher electron beam effective temperatures than the uncorrected fields. This is because the heating varies with the square of the error amplitude and inversely with the fourth power of the error spatial frequency. The corrected fields have much smaller amplitudes, but also much higher frequencies. Studies showed that although these error fields are quite large, they are smooth enough to permit even the highest energy electrons to adiabatically traverse them. Figure A7c shows such an adiabatic traversal of the field error by an electron, and Fig. A7d shows the amount of effective heating due to this perturbation as a function of the electron beam energy for an electron 1.25 cm from the axis of the solenoid.

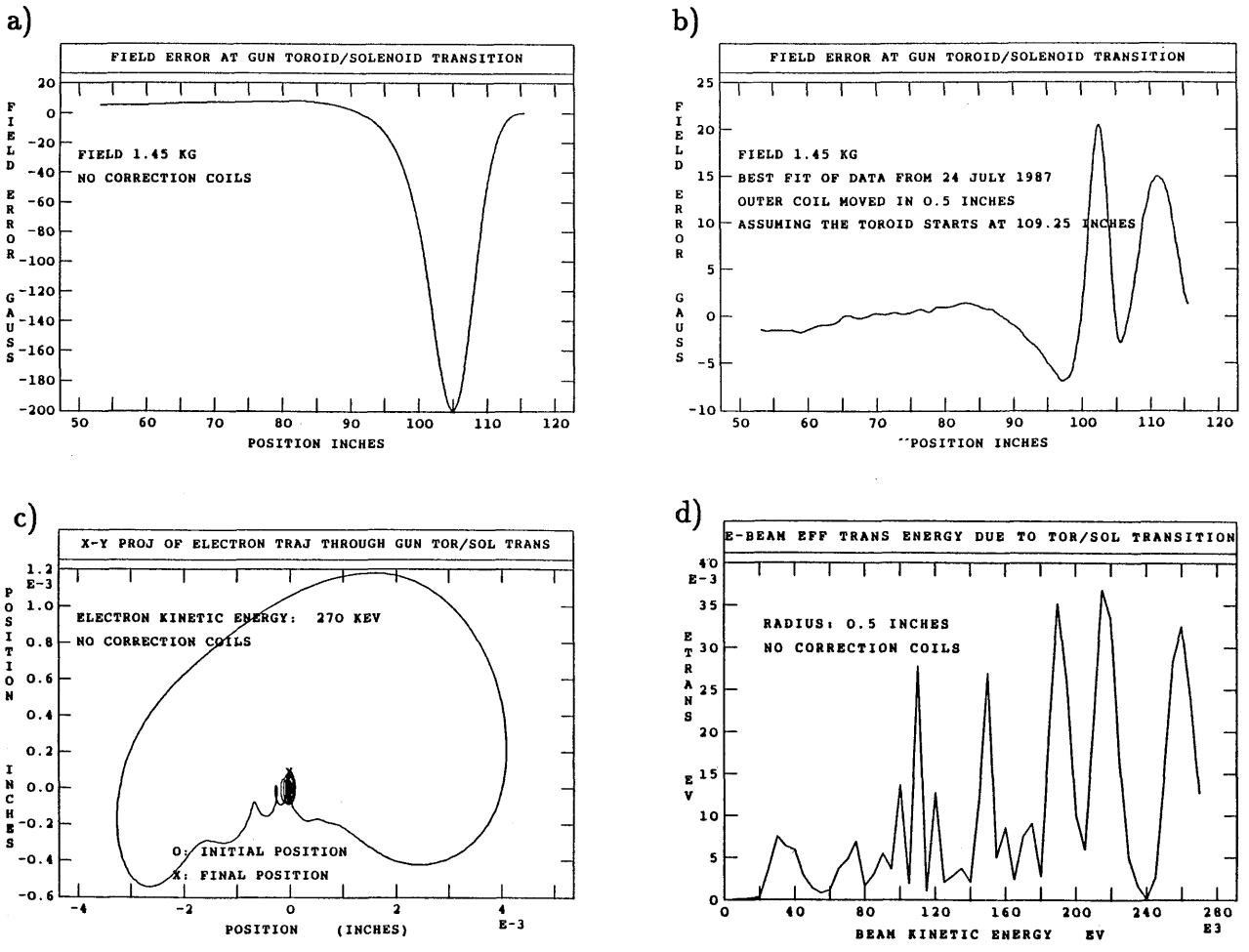

Figure A7. Magnetic field calculations. See text for explanation.

A.4.3 Collection Efficiencies

Typical collection efficiencies with no tuning are in excess of 99.9%. However, with very careful tuning, collection efficiencies as high as 99.995% have been achieved with 1 Amp of beam at low energies (25 keV). There are many parameters which can be varied to optimize the collection efficiency, many of which have not yet been explored. In the future, when times allows, we will perform systematic studies of the collector operation. An analytical model for predicting the collection efficiencies is also being developed, and this model will be compared with measurements.

A.4.4. Measured Properties of Cooled Proton Beams

Measurements of cooling were made with 45 MeV proton beams. The electron guide system magnetic field was 1.16 kG during these measurements. Much of our data on cooling is still preliminary. Below we present some of the results on longitudinal and transverse cooling and equilibrium beam properties.

• Equilibrium Energy Spreads: The cooled-beam momentum spread is measured by observing the coasting proton beam Schottky signal frequency spectrum. Both at 45 MeV and 148 MeV we observed cooled-beam energy spreads (FWHM) of about 2 keV, corresponding to momentum spreads of 2.2×10^{-5} and 7×10^{-6} respectively. Figure A4 shows such a Schottky signal for the very first cooling observed in the IUCF Cooler, and Fig. A8 is a spectrum showing the effect of an internal target. These energy spreads are equivalent in magnitude to the coherent shift in energy which we observe, which corresponds to a 1 V change in the electron cathode potential. The energy spreads are also about twice the minimum amount which one would expect due to the measured longitudinal drag rate and 60 Hz high voltage power supply ripple alone. Thus we appear to be in the position where increasing the electron beam current, and thus the longitudinal drag rate, may increase the time-averaged cooled-beam energy spread, though this has not yet been demonstrated. A ripple-bucking system which feeds the ripple voltage forward to an isolated electrode inside the cooling section is in place and should reduce the effect of this ripple by 1 to 2 orders of magnitude.

• Longitudinal Drag Rates: The longitudinal drag rate, the rate at which the electron beam can change the energy of a proton, has been measured in two different ways. One method involves exciting the electrodes which surround the electron beam inside the cooling section with a 50 to 100 V amplitude triangle waveform (much larger in amplitude than the

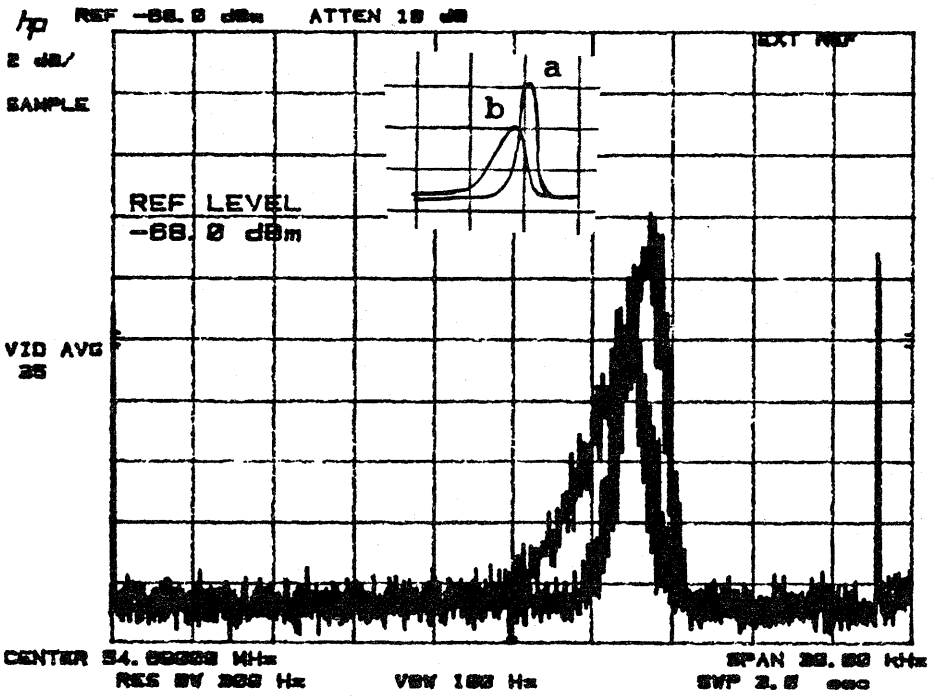

Figure A8. Schottky signals from a 45 MeV proton beam: (a) target off, (b) target on. The harmonic number is 53. RBW=300 Hz, CF=54.7 Mhz, 2 dB per division, 3 kHz per division. The target thickness was about 7×10^{13} N_2 atoms/cm^2.

60 Hz ripple on the high voltage power supply). The maximum frequency of modulation which the proton beam can track is then measured by observing the amplitude of the coherent Schottky signal frequency modulation, as shown in Fig. A9. These measurements were made using 45 MeV proton beams and electron beam currents of 0.4 and 0.22 A. The corresponding measured drag rates were about 215 keV/s and 130 keV/s, about twice the value we expected from estimates made using the nonmagnetized-theory and assuming the transverse electron beam temperature to be 0.2 eV.

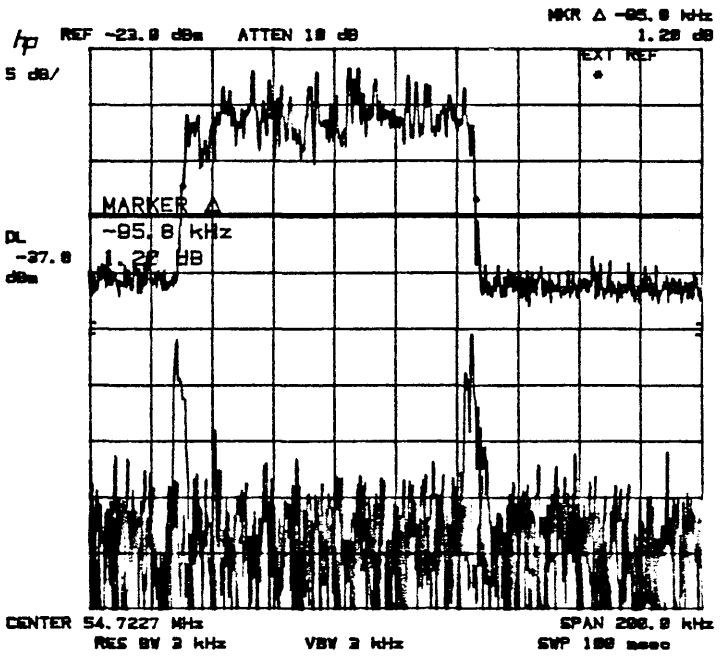

Figure A9. Longitudinal drag rate measurement. The lower trace displays the longitudinal Schottky signals with the drift electrode power supply at the two extreme voltages for calibrations. The upper trace, in peak hold mode, shows the extent of frequency modulation when the drift electrode power supply is ramping between the two extremes. For this particular frequency the proton beam was able to track the electron beam energy modulation.

The longitudinal drag rate can also be deduced by observing the rate at which the time spread of an rf bunched beam is reduced, as shown in Fig. A10. The incoming beam was bunched on the 9th harmonic of the fundamental revolution frequency, and the ring rf system was operated at the 6th harmonic; the electron beam current was 0.49 A, the rf cavity voltage 2 kV, and the ring transition energy is $4.85 \times Mc^2$. From this measurement we get a value for the rate of change in the amplitude of the synchrotron oscillations of about 120 keV/s, a value somewhat lower than the value obtained from the above set of measurements when the oscillatory motion is taken into account and the result is normalized with respect to the electron beam current. One important difference between the two measurements is that in the above set of measurements, the longitudinal drag rate was measured for a beam which had already been cooled transversely; whereas in this measurement, the ion beam had not yet been transversely cooled.

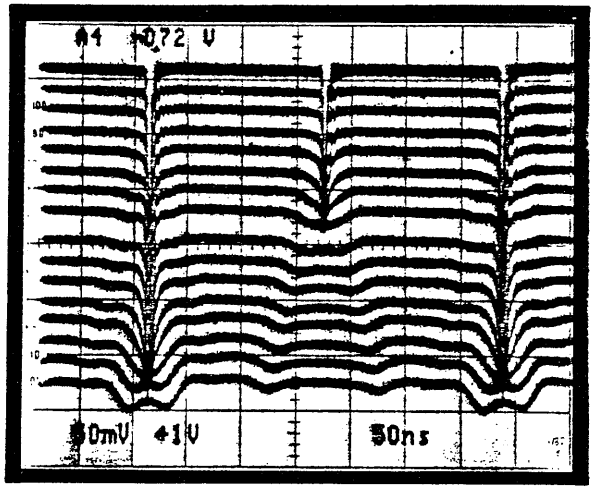

Figure A10. Display of beam microscopic time structure as the electron cooling system coalesces a beam bunched at h=9 into h=6 rf buckets. (0.132 s/trace, time moves upward).

• Transverse Cooling and Equilibrium: Transverse beam profiles were generated by sweeping the beam very quickly across a 7 μm diameter carbon fiber connected to the input of a high impedance amplifier, and detecting the current from knock-off electrons. The fiber is located in a high dispersion region of the ring, and the sweeping is accomplished by accelerating the beam with rf. The design lattice functions at this location are: η_x=4.15 m, and β_x=0.89 m. However, these lattice functions have not been measured at this location recently, and thus the calibration may be in error. Figure A11 shows the time evolution of the proton beam as measured by this beam diagnostic system. The equilibrium beam size corresponds to an emittance of less than 0.12π mm$\times$mrad (2σ), or a transverse temperature of about 0.35 eV in the electron cooling region where the beta functions are about 5 m. This measurement, however, only provides an upper limit on the equilibrium beam emittance. The measured beam size is also consistent with an equilibrium momentum spread which would result from less than a 1/2-least-significant-bit (2 V) mismatch of the electron beam energy with respect to the rf. The fiber is being moved to a region where the dispersion function is the same, but the beta function larger by a factor of about 5. This will allow us to reduce the upper limit of the proton beam temperature by the same amount.

No significant effects of intrabeam scattering were observed for proton beam currents ranging from 0.1 to 10 μA. Also, no significant change in the proton beam equilibrium was observed over the limited range of electron beam currents which we operated. The proton beam lifetime did increase linearly with electron beam current for a factor of two changes.

A.4.5. Conclusion

The performance of the IUCF electron cooling system thus far has been a delight to all. In the next year we are eager to operate the system over a much wider range of electron beam current and energy, making systematic measurements of the cooling forces and cooled beam properties. In addition, we will make a systematic study of the electron collector performance. We feel confident that the system will work as well for routine use in Cooler experiments as it has thus far in testing.

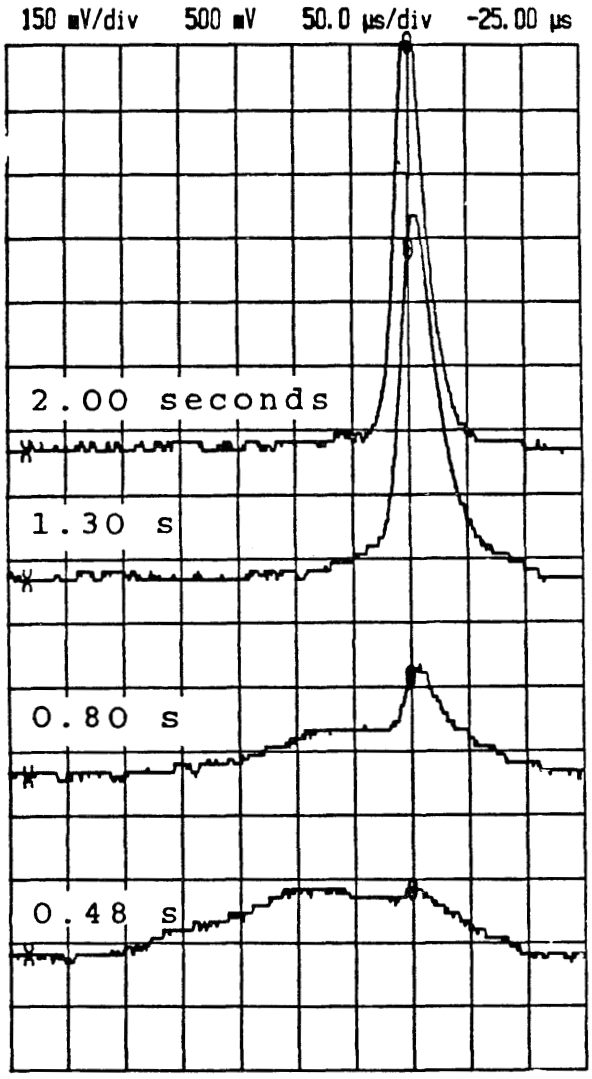

Figure A11. Transverse profiles of 45 MeV proton beam cooled with a 0.2 A electron beam. Profiles taken where $\beta_x = 0.89\text{m}, \eta_x = 4.15\text{m}$. This beam width has contributions due to energy spread as well as transverse emittance.

We are grateful for the very constructive communication we have had with colleagues building Cooler facilities at CERN, Uppsala, Darmstadt, Heidelberg, Jülich, and Tokyo.

A.5. Beam Diagnostic Systems, T. Ellison, M. Ball, P. Deckard, M. Fox, and D. Jenner

Cooler beam diagnostic systems[1] which have been under development for the last few years are now in operation. During the first few months of Cooler operation we were able to measure the Cooler beta functions, dispersion functions, chromaticity, and closed orbit; we could also measure the beam synchrotron frequency, tune, momentum spread, and emittance. In this report, the systems operation and performance are described. No analysis of the data, much of which soon becomes obsolete, is presented.

A.5.1 Measurements Made with the Beam Position Monitoring System

Cooler commissioning began using single-turn 45 MeV proton beams with intensities of about 200 nA. During this phase of commissioning the Beam Position Monitor (BPM) system allowed us to observe steering errors and transmission efficiency around the ring, as shown earlier in Fig. A2. This system also allowed us to observe focussing errors, as shown in Fig. A12, where the differences in the vertical position readings for the two settings of a vertical steerer, scaled by the ring design aperture, are plotted as a function of the design betatron phase. Simplistically, one could infer that there is a focussing error at the discontinuity in the phase advance of the oscillation, as shown in Fig. A2. However, the focussing errors are not necessarily the result of a single element and are therefore not so easy to locate in practice.

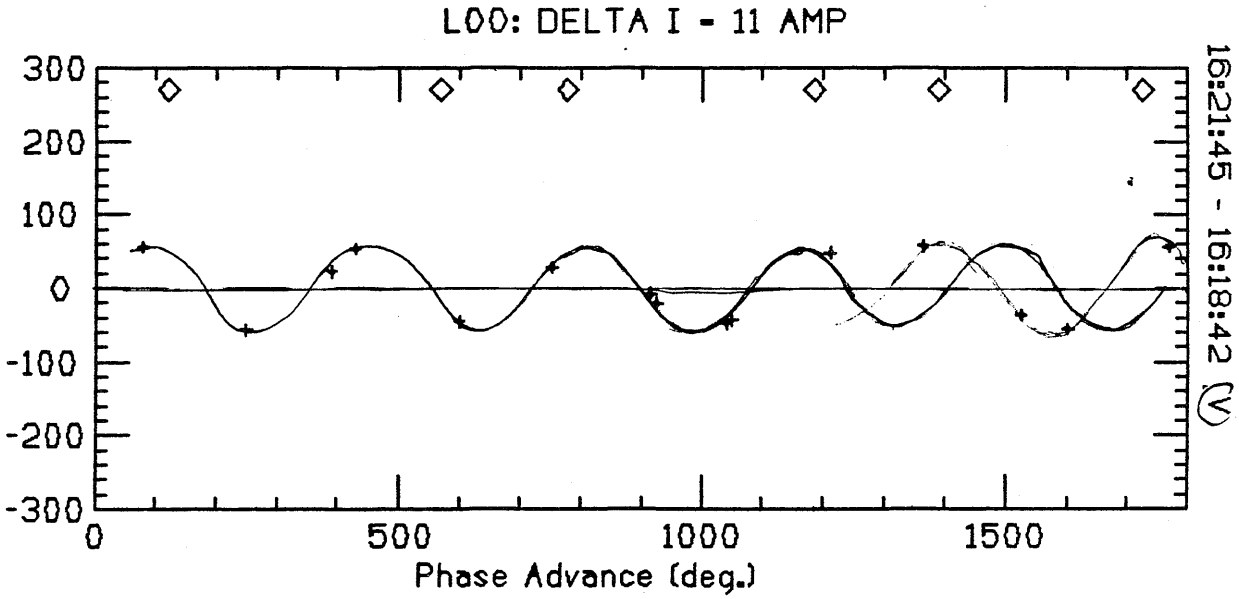

Figure A12. First turn vertical betatron oscillation due to an injection angle error. There is a discontinuity in the phase at about 1250°.

Once beam was stored in the ring, the BPM system was also used for measurements of the ring dispersion function, the beam transfer function, and for correction of the rf frequency program during acceleration.

Measurements of the dispersion function were made by frequency modulating the rf with a triangle waveform, thus modulating the beam energy in the same fashion. This results in a (measured) position movement of the same form proportional to the product of the (known) frequency deviation and the (unknown) dispersion function at the pick-up location. Such a measurement is shown in Fig. A3.

The transverse beam transfer function is measured using a network analyzer to non-destructively excite small transverse oscillations at a position electrode used as a kicker,

and monitoring the relative phase and amplitude of the oscillation at another electrode. This immediately results in a chromaticity measurement if we make the measurement at a low frequency, where the chromaticity is larger than the harmonic number of the betatron sideband carrier. (The beam momentum spread is separately measured using a spectrum analyzer and longitudinal Schottky signals.) Such a measurement is shown in Fig. A13, where the lower (slow wave) sideband was excited at the first harmonic of the beam revolution frequency. This year we will expand upon this system and use it to measure the betatron phase advance between all the pick-ups in the ring (numbering over forty).

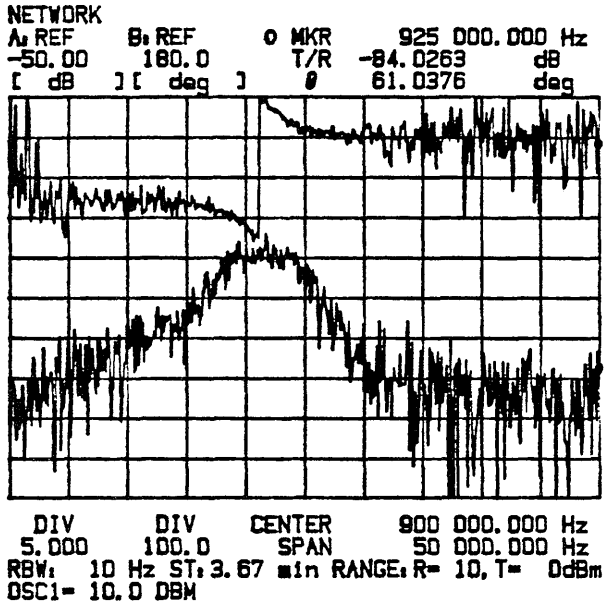

Figure A13. Beam transfer function measurement. The upper trace is the beam transverse oscillation phase (100°/div.) and the lower trace the oscillation amplitude (5 dB/div.) as a function of frequency. This measurement was made with a 45 MeV, 2μA proton beam.

This system also allows us to check the performance of steerer combinations designed to affect the orbit in only a localized portion of the ring. The successful operation of these local closed-orbit distortions also gives a check on the betatron phase advance between various steerers.

Figure A14 shows the primary beam diagnostic system used in tuning up acceleration. The upper trace is a logarithmic display of the beam intensity derived from the BPM system, and the lower trace is a display of the beam position at a location where the dispersion function is very large (4 m) and the beta function very small (0.5 m). The system automatically tracks the changing rf frequency keeping the signal within the extremely narrow (100 Hz) IF bandwith of the detector. This real time measurement allows very rapid alignment of the magnet and rf frequency programs. Figure A15 shows a similar plot, but on a much smaller time scale. Here the high bandwidth (up to 300 kHz) position detector was used to look at the early parabolic portion of the acceleration ramp.

A.5.2. Tune Measurement Systems

The betatron tunes have been measured using rf knockout, beam transfer function measurements, and by determining the betatron sideband frequencies of Schottky signals using a transverse resonant pick-up. All these techniques are capable of measuring the fractional tune to about three significant figures, a precision ten times greater than the

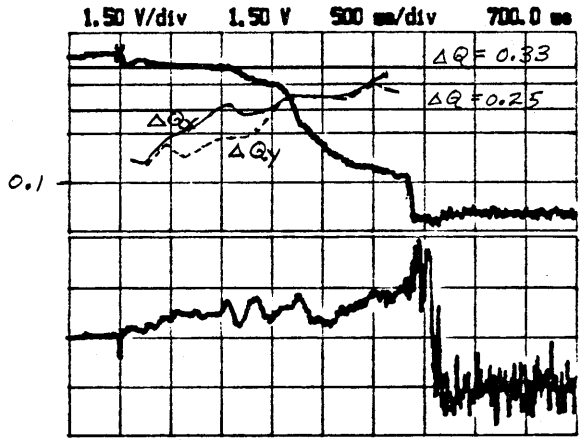

Figure A14. Display of beam current (15 dB/div., 20μA FS) and below a display of beam position (5 mm/div., 0 at center) during acceleration from 45 to 287 MeV. The beam is lost at about 250 MeV. The sketched-in lines show the transverse fractional tunes measured by rf knock-out. (0.1/div., 0 at bottom).

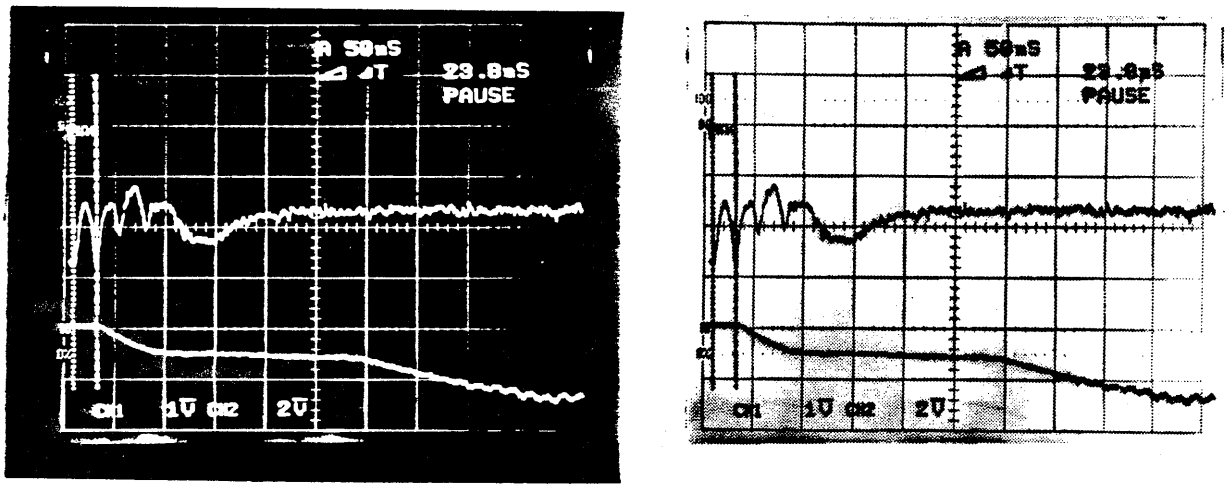

Figure A15. Oscilloscope traces showing (top) beam position (1.5 mm $\sim$ 0.04% Δp/p/div.) and (bottom) beam intensity ($\times$10/div) during the first few ramp vectors of acceleration.

uncooled-beam tune spread ($\Delta P/P \geq 0.05\%$) due to the chromaticity which has not yet been corrected. By measuring the tune change as a function of current changes in individual quadrupoles, the beta functions around the ring were also measured. When this data is complemented with phase advance data, a very good description of the Cooler lattice can be constructed.

A.5.3. Beam Time Structure Measurements

There are a number of longitudinal pick-ups for measuring the beam microscopic time structure. The BPM system spans the frequency range from 0.2 to 150 MHz with about 10 Ω/β coupling to the beam and input noise of 4 nV/$\sqrt{\text{Hz}}$. The low- and high-bandwidth wall gap monitors cover the range from 20-200 and 60-1300 MHz, respectively, with about

50 Ω coupling and input noise voltage of 0.5 nV/$\sqrt{\text{Hz}}$. The usefulness of the low frequency cutoff of the BPM system is evident in Fig. A10, which shows a beam bunched on the ninth harmonic (h=9) being cooled into h=6 buckets. Figure A16 shows the very high frequency response of the high bandwidth wall gap monitor. This system was very useful in early commissioning, giving instant feedback on the number of turns being made in the ring, and allowing us to measure the mismatch between the cyclotron and Cooler circumferences before coasting beam made frequency measurements possible.

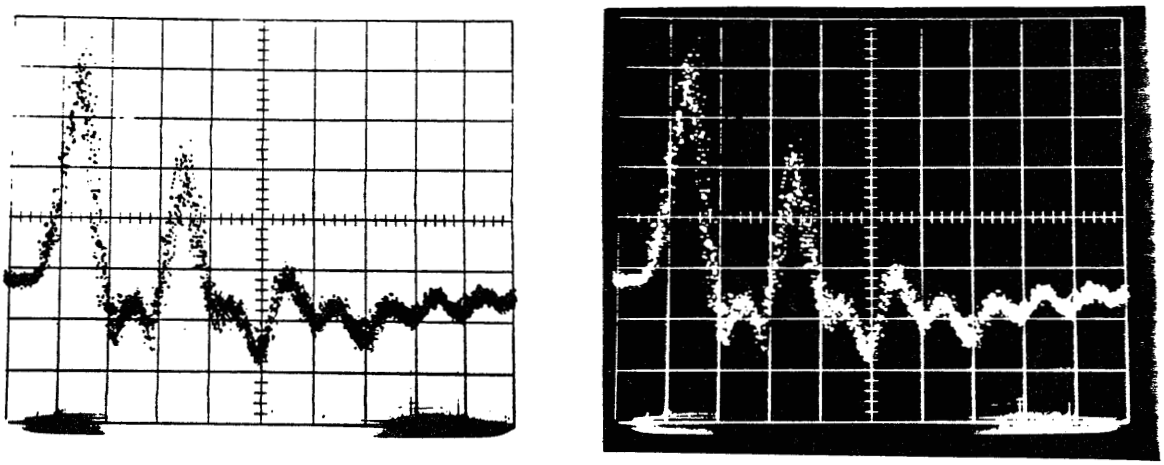

Figure A16. Sampled oscilloscope trace of cyclotron beam injected into the Cooler during an early commissioning run (1ns/div.). The second smaller trace is a beam pulse which has already gone once around the ring; this pulse has slipped in time by about 1.2 ns due to a 0.12% circumference mismatch between the Cooler and the cyclotron.

A.5.4 Resonant Schottky Pick-up

During the first phase of Cooler commissioning a combined vertical transverse and longitudinal resonant pick-up was installed. The pick-up consists of two parallel, shorted, $\sim$ 100 Ω transmission lines. The signals are "transformer" coupled into a 50 Ω system using small capacitors. The resonant frequency is varactor-tuneable over a 20% frequency range. The first (1/4 wavelength) resonance is at about 50 MHz. This style of pick-up nominally has a "zero" when the beam velocity is 0.33 c. Unfortunately, the majority of our operation the first year was with 45 MeV protons where v/c is 0.299. The pick-up still worked reasonably well at this beam energy, having an effective coupling impedance of 500 Ω, and input noise of about 0.5 nV/$\sqrt{\text{Hz}}$. In the electron cooling section of this report a number of longitudinal Schottky spectra from 45 MeV proton beams are shown. Figure A17 shows a cooled coasting (i.e. non-rf-bunched) beam intensity measurement made by recording the power in a longitudinal Schottky signal as a function of time. The resolution of this system ($<$ 10 nA) exceeds that of the best d.c. current transducers by 1 to 2 orders of magnitude. This summer a horizontal resonant pick-up will also be installed.

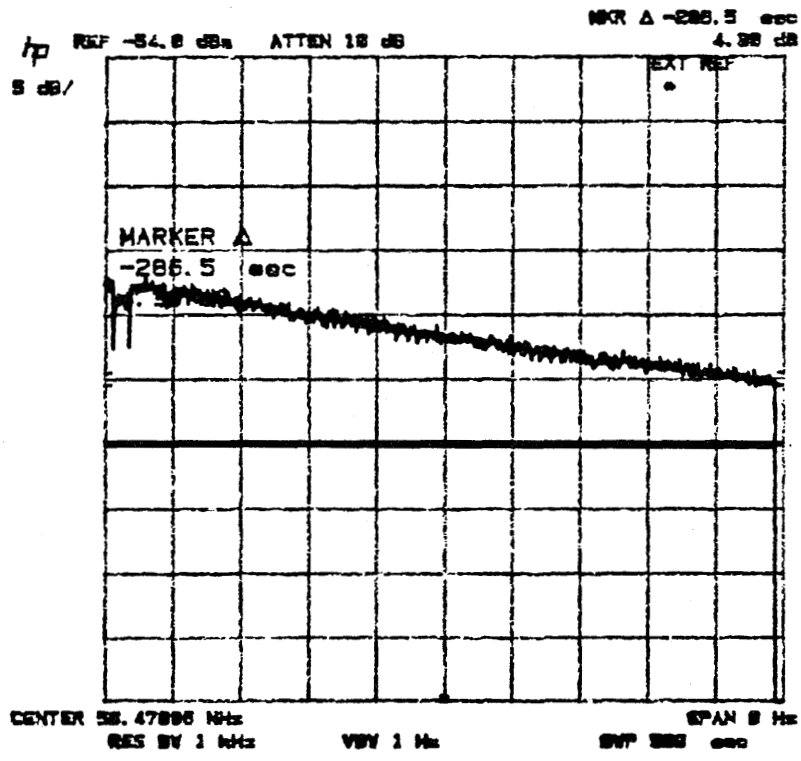

Figure A17. A measurement of power in a longitudinal Schottky band from an electron-cooled 148 MeV proton beam as a function of time on (5 dB/div., 50 s/div.). A 3 dB loss corresponds to a 50% in intensity loss. The injected current was 100 nA, and the noise level equivalent to 6 nA.

A.5.5. Beam Profile Measurements

A very simple beam profile measurement system was built to measure the transverse cooling rate and equilibrium emittance of the stored beams in the Cooler. The system consists of a high impedance, high bandwidth FET-input op-amp connected to a 7 μm carbon fiber mounted vertically in a high dispersion (4 m), low beta (0.9 m) region of the ring. The beam is moved across the fiber by modulating the rf frequency with a ramp waveform, and the current due to electrons knocked out of the fiber is measured. In order to calibrate the monitor it is necessary to know the time-derivative of the frequency and the dispersion function at the monitor; and in order to convert the measured beam profile into an emittance or temperature, it is necessary to know the beta function at this location. In the future, these lattice parameters will be measured accurately using the systems described above. Figures A11 and A18 show the output of this detector during a measurement of a cooled 45 MeV proton beam.

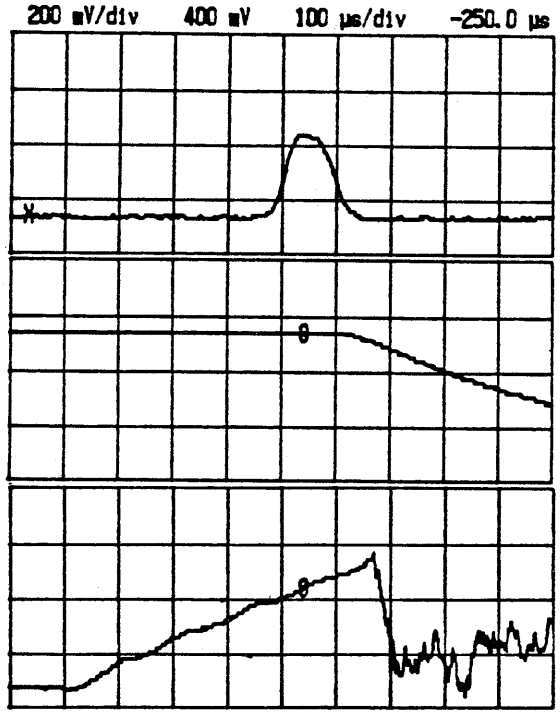

Figure A18. Beam profile measurement. The upper trace is the current emitted from the 7 μm carbon fiber; the center trace a linear plot of beam intensity, and the lowest trace the beam position, where small (8 kHz) synchrotron oscillations are observed. The beam is destroyed after the measurement. The beam current was a few μA.

A.5.6. Cyclotron Diagnostic Systems

A few cyclotron diagnostic systems are also under development, including a new cyclotron beam phase probe, beam timing system, beam position electrode amplifier, intensity monitor, and buncher phase modulator.

The new buncher phase modulator system and cyclotron beam intensity detector have been put into operation and are described fully in the cyclotron operation section of this report.

A.5.7. Conclusion

At IUCF we are developing a large amount of expertise in building beam diagnostic system hardware. However, we are still learning how to make various measurements and how to use these measurements to improve the performance of our accelerators. In addition, not all the present systems are under computer control. Ultimately we would like to implement computer-controlled measurement, analysis, and machine modification based upon these measurements. As a first step in this direction, the Electronics Division has obtained a work station and the PLUS software system.[2] In the upcoming year, we plan to implement this system in the Cooler to analyze closed-orbit and focussing errors using computer-acquired data from the BPM system. Thus, in the future, the emphasis of the Beam Dynamics Group will be on analyzing the performance of the accelerators and interfacing diagnostic systems to the computer, so they are easily accessible to the operators, as well as on developing new hardware.

1. T.J.P. Ellison, C.M. Fox, S.W. Koch, Nucl. Inst. and Meth. **B24-25**, 873 (1987).
2. M. Lee, S. Clearwater, E. Gheil, and V. Paxson, in Proc. of the 1987 Particle Accelerator Conf., (Washington, DC, 1987) p. 611.

A.6. Controls, B. Manwaring and J. Graham

This year has seen the completion of a major Controls project: controls for the Cooler Synchrotron/Storage Ring. This project involved a new controls computer (PLUTO), a high-speed multiplexing system, 250 readouts, 150 DAC outputs, a fiber-optics serial link to a 300 KV terminal, and a programmable-controller-based vacuum system. In addition, we were for the first time forced into the realm of periodic phenomena: from control of an essentially DC cyclotron, we have moved to a machine with 100-odd ramped power supplies linked to a master timing system.

• Ramping: To handle ramping, the 'RAMPDAC function generator' card was developed at IUCF over a two-year period. This card uses vectors, specified by slope and endpoint, to approximate an arbitrary ramping waveform. Eight independent ramps of 256 vectors each can be stored on any card. The card's analog output is from a 16-bit optically-isolated DAC which can be directly wired to a Cooler Ring magnet power supply. When the ring is not functioning in its synchrotron mode, the RAMPDAC cards function as simple computer-controlled DACs with the vector-generation circuitry disabled.

At present, 96 RAMPDAC cards are installed and working. These cards and their associated power supplies and control electronics occupy two 19-inch racks. Each card is roughly 7 × 9 inches and contains 50 chips; twelve of these cards mount in an Augat 'R-series' bin. A system of four fast 16-bit ADCs has been installed to permit automated testing of the RAMPDAC array. Each ADC is multiplexed, via mercury-wetted relays, to 24 RAMPDAC card outputs. This system can detect dropped bits, and can also sample a ramp in progress for graphics display at the console.

• Timing: A visitor from Brookhaven alerted us to the Jorway 221/222 Camac timing module, which provides twelve programmable timing signals with a resolution of 0.1 microsecond. One such module, coupled with a bin of NIM electronics, presently provides all ring timing, including injection pulses, scope and analyzer triggers, computer interrupts, splitter magnet control (for beam splitting). We envision three Jorway modules (36 programmable outputs) in the long run, as hardware takes over complete ramp control, as well as interface to the experimentalist.

• Multiplexer: To maintain compatibility with the Cyclotron Control System, a system of memory-mapped input and output ports was developed. This system performs 16-bit word transfers from the Controls Computer Q-bus in about a microsecond over a parallel differential driver/receiver bus. Its I/O signals are identical to those of the Cyclotron, which enabled us to use a good deal of already-developed electronics and software in the new system. The main use has been for readouts (250 installed) and non-ramping DACs (55 installed).

• Console: Two of our standard consoles are installed in the Cooler building under the control of PLUTO. Each console consists of a color monitor, monitor page select buttons,

two DAC control knobs, two levers, a trackball, and a select button. In addition there is a medium-resolution graphics display. In the long run, Ring control will be from the main control room, but these local consoles will be invaluable for testing and development.

A.7. Cooler Control System Computers, J.C. Collins

While 1987 was the primary year in which to prepare for Cooler commissioning, some work did get done on DIANA, the cyclotron control computer. The on-line device database was consolidated from three separate files (an historical artifact) into one, simplifying access and maintenance. Tools were installed to allow the operator to construct and maintain pseudo-devices, called *Combos*, each consisting of some number of real devices. A change in the *Combo* "DAC value" modifies the DAC of each associated real device by an amount related to the product of the *Combo* change and an operator-specified coefficient for that real device. Cooperating programs which communicate via DECNET were installed on both DIANA and data acquisition VAXen to offer experimenters control of some devices. For operational reasons, only a very limited list of devices are accessible in this fashion. Even so, K600 spectrograph users benefit greatly from this utility. The steering loop control program was greatly expanded to include use of the Beam Position Monitors (BPMs), developed originally for the Cooler, but installed in some cyclotron beamlines, and to allow for greater user interaction with the loop parameters. Finally, a software project was started to give the operator access to TRANSPORT calculations from a VAX using current beamline parameters, for diagnostic and tuning purposes.

PLUTO, the Cooler control computer, was the focus of most of the new development work of 1987. The computer, an LSI-11/73 running RSX-11M-PLUS on 1 MB memory and a single 32 MB disk, was installed in the Cooler control area, along with two operator stations and a medium resolution (768 $\times$ 574) graphic display. The operator station software, started in 1986, was completed, the basic acquire/control function resident library was installed and actual ADC readout and DAC control were demonstrated, allowing the Cooler ring to be run in "storage" mode.

After ramping DAC cards were installed, primitive ramp control functions were added to the acquire/control resident library and debugged. By the end of the year, an interactive ramp generation program was used to ramp the main dipole through a fill-ramp-run-reset cycle.

For "storage" mode operations, a graphic BPM display program set was written to show horizontal and vertical beam positions simultaneously with intensity measurements for the 36 extant BPMs. The *Combo* facility from DIANA was expanded and modified to allow recursive calls: *Combos* of *Combos*. A utility was created so that operators can save all DAC and ADC values, compare them to saved and/or current values and restore DACs from any saved set. All functions can be performed on all or on predefined subsets of devices. DECNET was used to connect the acquire/control resident library functions in DIANA and PLUTO in as transparent a fashion as possible. (Total transparency was not possible because acquire/control library functions via DECNET require four to five orders of magnitude longer to complete than normal functions.) This made it possible to control all cyclotron devices from the Cooler operator stations and all Cooler devices from the cyclotron stations.

The Cooler electron beam 300 kV platform is controlled by a standalone Motorola M6809-based system called LUCIFER. The control software is done entirely in assembly level language, cross-assembled on an IBM PC. This system performed flawlessly, beginning with the first operation of the electron cooling system. Work also began on software to control the Cooler bakeout system. This code is being written in TURBO PASCAL to run on an IBM PC.

A.8. The Cooler Electron Terminal Fiber-Optic Control Link, J.R. Graham

Control hardware for the high-voltage electron terminal and associated power supplies was installed in December, 1987 and January, 1988. Complete remote control of the electron terminal power supplies via the control console was accomplished in February, 1988. In order to control the devices inside the electron terminal, it was necessary to provide some type of electrical isolation between the terminal and the control computer. As a result, a microprocessor controlled fiber-optic serial data-link was developed. The 'link' consists of two microprocessor controlled serial interfaces, one on each end, connected by a 52 meter duplex fiber-optic cable. A block diagram of this system is shown in Fig. A19.

Serial NRZ data transfer rate is 1.0 Mbps. Maximum computer thru-put is approximately 100 Hz. This means that the control computer can send commands to the link at a rate no faster than 100 times per second. If this rate is exceeded, the link will generate a "System Overrun" message and then continue with normal operation.

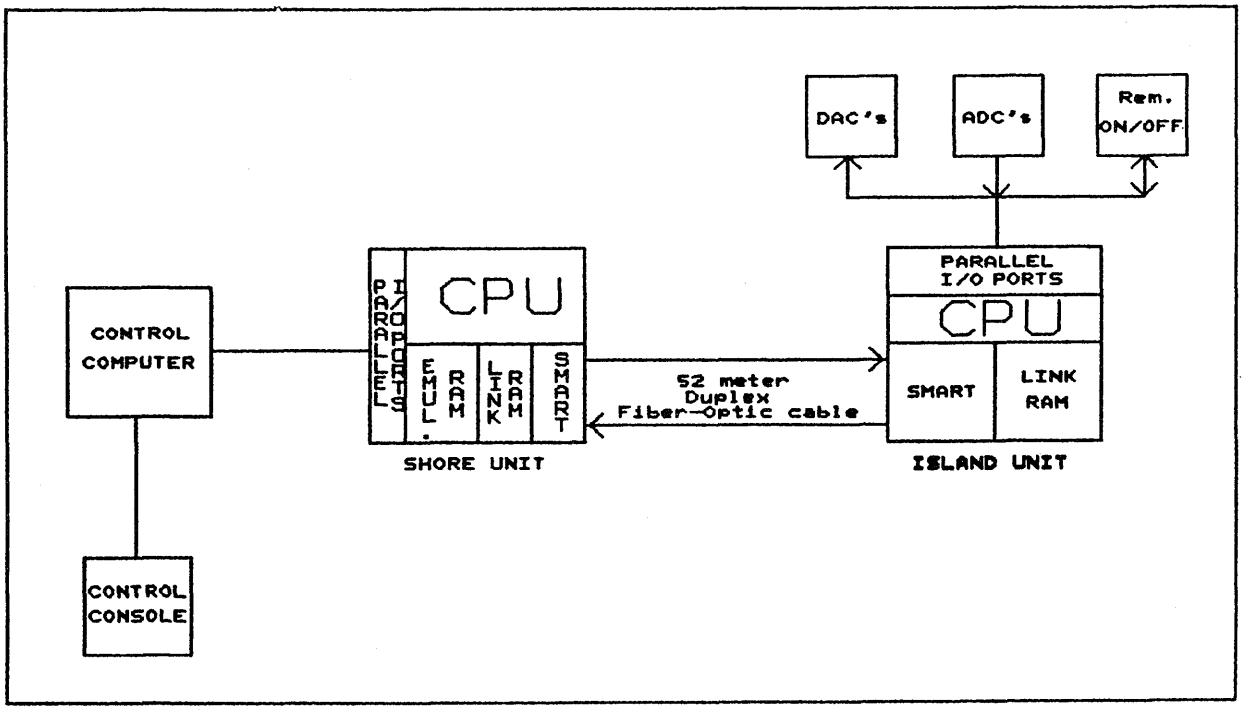

Figure A19. System block diagram.

Serial data is transferred in packets up to 32 words in length. The first word consists of a "command word" if the data direction is from ground-to-terminal or a "status word" if the direction is from terminal-to-ground. Another word in the packet is responsible for maintaining proper handshaking with the other end. The remainder of the packet consists of various data for writes to digital-to-analog converters, reads from analog-to-digital converters, or writes to and reads from a remote-on interface.

The versatility of this system lies in its use of the "S.M.A.R.T." IC, sold by Standard Microsystems Corporation. "S.M.A.R.T." stands for "Synchronous Mode Avionics Receiver Transmitter". This chip utilizes the COM1553B serial communications standard. It contains on-chip DMA as well as error checking.

Because of the integral communications error checking, it is relatively simple to handle various types of communications errors such as invalid data, missing data, or improper remote terminal addresses. When an error occurs, a message is displayed at the unit experiencing the problem. If the error is serious, the S.M.A.R.T. may actually go into an undefined state. If this happens, the software will eventually detect the error and force the S.M.A.R.T. to recover. Most errors are not serious and will receive only passing notice by the software.

Each end has a block of dual-port memory, one port accessed by the MPU and the other port accessed by the S.M.A.R.T. This is the "Link Ram" shown in Fig. A19. In this way, the MPU may process data which is periodically moved by the S.M.A.R.T.

Figure A20 is a map of this dual-port memory. The first two locations always contain the command control code and word for the S.M.A.R.T. The remainder of ram is available for data storage by the MPU and S.M.A.R.T.

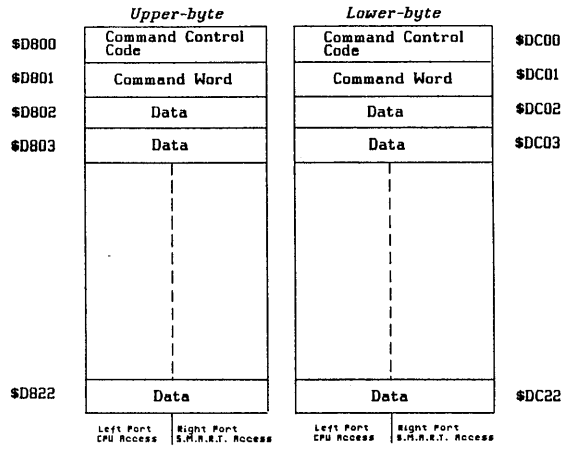

Figure A20. Map of "S.M.A.R.T." dual-port memory.

Figure A21 is an address map of the Shore unit. Notice that the Shore unit contains two blocks of RAM. One block is the RAM shared by the MPU and the S.M.A.R.T. The other block is shared by the MPU and the main control computer. This latter block contains data received from analog-to-digital converters, and remote on/off status information. By default, data transferred between Shore and Island units is stored here.

Whenever an operator desires to change the value on a digital-to-analog converter, the main control computer will interrupt the Shore MPU, sending it a command to write

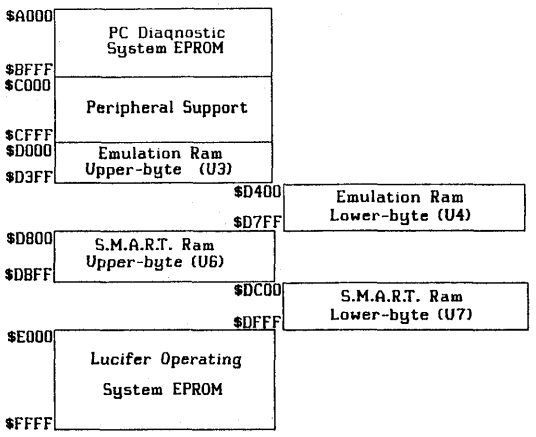

Figure A21. An address map of the shore unit.

to a DAC. The MPU will read the desired DAC data from the control computer, put it in the the Link RAM, and strobe the S.M.A.R.T., initiating a data transfer to the Island unit. Once data is successfully received by the Island unit, the Shore unit continues with its default transfer mode. Handshaking is provided so that any memory access by the S.M.A.R.T. halts the MPU. Consequently, the MPU may "steal" the data bus between S.M.A.R.T. accesses.

The S.M.A.R.T. in the ground side of the link is called the "bus controller" and in the electron terminal, the "remote terminal".

An example of a typical data transaction is described here. Assume we will transfer a data word to a digital-to-analog converter in the electron terminal.

1. The bus controller transmits a serial packet to the remote terminal in the following form:

Location within packet	Data
00	Command word
01	DAC data word
02	DAC data word
30	DAC data word

2. The remote terminal responds by sending the following packet back to the bus controller:

31	Status word

Although the Shore and Island units each have eight buttons on the front panel, only one on each unit is currently used. The button is labeled "RS-232", and is located next to a 25-pin DB connector. If a serial terminal, such as an IBM-PC , with appropriate communications software is connected to this port, and the button is momentarily depressed, Lucifer's "Remarks" display will indicate "Monitor Activated". On the terminal screen the prompt "Lucifer>" will appear. This tells us that we are now in the position to directly

read any addressable location. We may modify any writeable address as well. If we choose to execute a particular address, we need only to enter the appropriate single-character command, along with the desired address.

A very useful feature of this monitor is that we may upload a file of hex bytes from the IBM to the unit that we are attached to. This allows us to assemble test routines offline and then upload them for execution.

As of this writing, the link has been online since February of this year and has yet to fail or produce any type of communications errors.

A.9. The Cooler Ring Power Converters, T. Bertuccio

The Cooler ring and associated beam line magnets are powered by approximately 125 power converters. Each converter contains regulation circuitry to maintain the output current at precisely the value commanded by a digital to analog converter. The chain of ring main dipoles and quadrupoles requires static stability tolerances of 5 and 20 ppm, respectively, and dynamical tracking tolerance of 300 ppm.

The type of power converter specified for this project was the conventional series pass transistor regulator that employs a dissipative bank of power transistors between a rectified-filtered source of "raw d-c" and the stabilized output. The higher-powered converters for the dipoles and quads have a variable AC input level to minimize pass bank dissipation losses. The dipole converter AC input is dynamically changed during ramping via a multitap transformer tap changer employing SCR's whereas the quadrupole converters AC input level is preset and remains fixed.

All the power converters were procured from commercial vendors and employed an output capacitor to control the roll-off of the gain versus frequency characteristic which establishes the stability margin of the current control loop. This conventional design method, however, proved to be unworkable with the quadrupole network which has multiple converters hooked up to separate windings on a common magnet yoke for each quad. Thus multiple converters are interconnected to one another via transformer coupling. To eliminate the interaction between converters driving a common load the output capacitors had to be removed, which in turn necessitated a major reworking of the control loop stabilization networks. A Venable System 350 frequency response analyzer was employed to (a) measure under actual closed-loop operation the open-loop gain-phase characteristic of each converter regulation loop and (b) establish the compensation network values necessary to achieve an adequate phase and gain margin for the regulator.